CH₄ emissions from Northern Europe wetlands: compared data assimilation approaches

Guillaume Monteil^{2, 1}, Jalisha Theanutti Kallingal¹, and Marko Scholze¹

¹Department of Physical Geography and Ecosystem Science, Lund University, Lund, Sweden

Correspondence: Guillaume Monteil (guillaume.monteil@bsc.es)

Abstract. Atmospheric inverse modelling and ecosystem data assimilation are two complementary approaches to estimate CH₄ emissions. The inverse approach infers emission estimates from observed atmospheric CH₄ mixing ratio, which provide robust large scale constraints on total methane emissions, but with poor spatial and process resolution. On the other hand, in the ecosystem data assimilation approach, the fit of an ecosystem model (e.g. a Dynamic Global Vegetation Model, DGVM) to eddy-covariance (EC) flux measurements is used to optimize model parameters, leading to more realistic emission estimates.

Coupled data assimilation frameworks capable of assimilating both atmospheric and ecosystem observations have been shown to work for estimating CO₂ emissions(e.g. Rayner et al. (2005)), however ecosystem data assimilation for estimation CH₄ emissions is relatively new. **Eallingal et al. (2024a) developed the GRaB-AM data assimilation system, which performs a parameter optimization of the LPJ-GUESS against eddy-covariance estimation of CH₄ emissions. The optimization improves the fit to EC data, but the validity of the estimate at large scale remained to be tested.

In this study, we used confronted CH₄ emissions optimized using the GRaB-AM system to atmospheric CH₄ observations and to emission estimates from the LUMIA regional atmospheric inversion system (Monteil and Scholze, 2021)to confront wetland emissions from. We found that the two approaches lead to very consistent corrections to the prior emission estimate from natural wetlands, with roughly a halving of the annual total compared to the LPJ-GUESS prior. Our findings confirm the interest of the GRaB-AM approach to atmospheric CH₄ measurements in Europe. We then perform inversions using the information from GRaB-AM as prior. This let us infer a refined estimate for wetland emissions in Nordic Europe, and to explore the potential for a fully coupled data assimilation frameworkconstrain the contribution of natural ecosystems to the total methane budget, which is difficult to achieve for atmospheric inversions outside regions where emissions from natural ecosystems clearly dominate the emission budget.

20 1 Introduction

Methane (CH₄) is the second most important greenhouse gas after CO₂, accounting for around 21% of the total effective radiative forcing of the well-mixed greenhouse gases (Forster et al., 2023). Its presence in the atmosphere has more than doubled since pre-industrialization era, with background mixing ratio at Mauna-Loa approaching the 2000 ppb (1931.91 ppbv in April 2024, according tohttps://gml.noaa.gov/ccgg/trends_ch4 (last consulted: September 2024). After a stabilization from

²Barcelona Supercomputing Center, Barcelona, Spain

1998 to 2007, the atmospheric CH₄ concentration has started increasing again, at an accelerating pace. Although several recent studies attribute this renewed increase mainly to anthropogenic emissions (Nisbet et al., 2016; Thanwerdas et al., 2024), an important contribution from wetlands has also been proposed (Qu et al., 2022; Peng et al., 2022; Christensen, 2024). While for the global <u>natural</u> methane budget, tropical wetlands are most important, Arctic wetlands could constitute a potent positive climate feedback (Zhang et al., 2023) and there are indications that their emissions have been increasing in recent years (Yuan et al., 2024; Ward et al., 2024).

Emission estimates for natural wetlands can be obtained through process models, which calculate methane emissions according to various environmental inputs (meteorological forcings, soil type, hydrology, etc.). The model simulates or approximates known physical processes with various degrees of complexity. However, uncertainties on the existence or the importance of specific processes, lack of accuracy of some parameterizations, combined with the high non-linearity of the models leads to large differences between the estimates at large scales. For example, a comparison of mean annual CH₄ emissions from 16 models used in the Global Carbon Project (GCP) has shown that global estimates range from 118.7 TgCH₄/year to 195 TgCH₄/year (Ito et al., 2023). Specifically for wetlands above 15°N, the estimated emissions ranged between 10.5 TgCH₄/year (SDGVM model) and 40 TgCH₄/year (ORCHIDEE). Similar ranges were also found during the WETCHIMP model intercomparison project (Melton et al., 2013), which reported a ±40% spread of the estimates around the all-model mean of 190 TgCH₄/year, for global emissions.

The Global Rao-Blackwellized Adaptive Metropolis (GRaB-AM) approach developed by ? is a data assimilation (DA) Kallingal et al. (2024a) is a parameter estimation data assimilation system based on Bayesian statistics, in which parameters of the LPJ-GUESS model connected to the production, transport and oxidation of CH₄ pathways are adjusted to optimize the model fit to eddy-covariance flux measurements. The optimized parameters can then be used to produce a gridded estimate of the methane emissions, which combine the process knowledge embedded in the LPJ-GUESS model with the added information from in-situ flux observations. However, the quality of the resulting emission estimate remains difficult to formally assess. The optimization is done by performing site-scale simulations, with local measurements of meteorological forcings and a good knowledge of the wetland types and their spatial distribution. Scaling up to Northern hemispheric emissions is then done using forcings from meteorological reanalysis, with hypothesis on the wetland type and fractions in each grid cell, which carry their own uncertainties. Total CH₄ weltands emissions for the region north of 45°N as simulated by LPJ-GUESS model (posterior) 43.09 TgCH₄/year for the uncalibrated (prior) model and 37.54 TgCH₄/year for the calibrated LPJ-GUESS model (posterior) (?)(Kallingal et al., 2024b).

An alternative approach is to infer methane emissions from their observed impact on atmospheric CH₄, using inverse modeling approaches (Houweling et al., 2017). Atmospheric inversions Inversions leverage the fact that atmospheric observations are sensitive to the emissions aggregated over a large area, owing to the long lifetime of atmospheric CH₄, and therefore can provide large-scale constraints on methane emissions. However, this also means that the observed atmospheric methane concentrations are the result from a mixture of emissionsprocesses. The This approach has been used by several recent studies to estimate emissions from arctic wetlands (Wittig et al., 2023; Tsuruta et al., 2019; Ishizawa et al., 2023). However, observations of atmospheric CH₄ are sensitive to the net methane emissions, which limits the capacity of inversions to

independently constrain emissions from a specific source is therefore limited to cases where there is a distinct spatial and/or temporal emission pattern that can be used to isolate the contributions of that process to the net methane emissions. Emissions from natural wetlands dominate the methane emission budget in the arctic region, which has been used by several recent studies to derive inversion-based estimates of arctic wetlands (Wittig et al., 2023; Tsuruta et al., 2019; Ishizawa et al., 2023) resolve wetland emissions independently from other CH₄ sources. Satellite observations, such as TROPOMI XCH4 retrievals (Nesser et al., 2024; Tsuruta et al., 2023), or retrievals from the upcoming CO2M (Sierk et al., 2021) or MERLIN instruments (Ehret et al., 2017), can help increase the resolution of inversions, but their coverage is not constant (cloudiness, short day length at high latitudes in winter, etc.), and their signal-to-noise ratio is lower than that of in-situ observations for detecting emissions (because satellite XCH₄ retrievals quantify the column-averaged CH₄ mixing ratio, therefore they incorporate a stronger background contribution than surface observations). Some implementations of the inverse approach use observations of the isotopic composition of atmospheric methane (δ¹³C-CH₄, δD-CH₄) as an additional constraint on the source process distribution (Basu et al., 2022; Thanwerdas et al., 2024; Drinkwater et al., 2023), but the low amount of available data and the uncertainties on the isotopic signatures of methane emissions have limited the practicality of that approach.

The inverse and DA atmospheric inversion and parameter estimation approaches assimilate complementary observations, and there could be a is potentially a strong benefit in integrating them further in a unified CH₄ data assimilation system, on the model of what exists for CO₂ (Rayner et al., 2005). In this study, we take a step in that direction by confronting emissions estimates from the GRaB-AM data assimilation system of ? Kallingal et al. (2024b) to inverse modelling estimates from the LUMIA (Lund University Modular Inversion Algorithm) regional inversion system Monteil and Scholze (2021), focusing our analysis on high-latitude European wetland emissions. The confrontation between the approaches serves both as a form of cross-validation, but also to explore the potential for a joint data assimilation setup.

80 2 Methods

90

We compare four main wetland emission estimates: two LPJ-GUESS, one from the default setup (LPJ-GUESS-unopt) and one from the GRaB-AM optimized setup-GUESS (LPJ-GUESS-opt), and two LUMIA inversions, using these LPJ-GUESS simulations, and their uncertainties as prior: LUMIA-Lprior (using LPJ-GUESS-unopt as prior) and LUMIA-Lpost (using LPJ-GUESS-opt as prior). These four simulations correspond respectively to a pure bottom-up estimate, a flux-observation informed estimate, a atmospheric observation informed estimate, and an estimate informed both by flux and atmospheric data. Two additional LUMIA inversions were performed as sensitivity simulations (LUMIA-Lprior+corr, LUMIA-Lpost+corr), with a different prior error covariance structure (see also Section 3.1). The supplementary figures also include some results from an additional sensitivity test, LUMIA-Lpost_total, in which only the total CH₄ emissions (wetland + non-wetlands) was optimized.

The study covers the year 2018, for the LUMIA inversion domain represented in Figure 1, although we focus mainly on the observations in the Nordic sub-domain (red box in Figure 1). The domain extent is based on that of a CH₄ regional inverse

modelling intercomparison, jointly organised by WMOs Integrated Global Greenhouse Gas Information System (IG3IS) and the Horizon-Europe CoCO2 project (https://coco2-project.eu, last consulted: 23/09/2024), to which this study contributes.

2.1 Wetland emissions modelling

2.1.1 LPJ-GUESS

100

105

115

120

LPJ-GUESS is a dynamic global vegetation model (DGVM), designed to simulate the interactions between vegetation, soil, and their responses to environmental changes and management (Sitch et al., 2003; Smith et al., 2001, 2014). The model can simulate vegetation dynamics, carbon and water cycles, and soil biogeochemistry from local to global scales, including the simulation of methane fluxes from natural wetlands.

For this study, we used the Arctic-enabled version 4.1 of the model (Smith et al., 2014), which differs from previous versions for having detailed representation of wetland CH₄ emission. The process descriptions of the CH₄ module were mostly adopted from the LPJ-WHyMe model (Wania et al., 2010), and are described in detail in (McGuire et al., 2012). It is based on a "potential carbon pool", which is then decomposed to soil organic carbon distributed vertically in the soil layers. Methanogens use this decomposed organic carbon and produce CH₄. A part of this produced CH₄ gets oxidized by O₂ and the remainder is transported to the atmosphere by diffusion, ebullition, or plant-mediated transport (see Wania et al. (2010); ? Wania et al. (2010); Kallingal et al. (2024a) for more details). The model is driven by daily climate data including air temperature, precipitation, and shortwave radiation taken from the Climatic Research Unit-Japanese Reanalysis (CRU-JRA; Harris et al. (2020) dataset. Annual atmospheric CO₂ concentrations, as additional model input for LPJ-GUESS, are obtained from the Global Monitoring Laboratory (https://gml.noaa.gov/ccgg/trends), and the soil property data was extracted from WISE5min, V1.2 Soil Property Database (Baties, 2005).

Model simulations covering the area north of 45°N are produced using PEATMAP (Xu et al., 2018), which combines geospatial information from various sources to create a global map of wetland extent. PEATMAP has been used in several studies mainly because it is an updated quantification of peat land extend, and it focuses on mapping peatlands, such as marshes and swamps, which are the dominant wetlands in northern latitudes (Peltola et al., 2019; Aalto et al., 2024; Müller and Joos, 2020).

2.1.2 GRaB-AM flux data assimilation framework

To optimize the methane module of LPJ-GUESS, ?-Kallingal et al. (2024a) developed the GRaB-AM data assimilation framework, which seeks to optimize the value of ten highly sensitive parameters in the methane module of LPJ-GUESS (connected to production, transport and consumption pathways of CH₄), based on the model fit to eddy-covariance (EC) flux observations. The minimization is performed using an adaptive scheme of the Markov Chain Monte Carlo Metropolis-Hastings algorithm (Metropolis et al., 1953; Hastings, 1970). In ?Kallingal et al. (2024b), observations from 14 natural wetlands distributed across the Northern Hemisphere above 40° and over a total period of 20 years (from 2000 to 2020 with individual sites contribut-

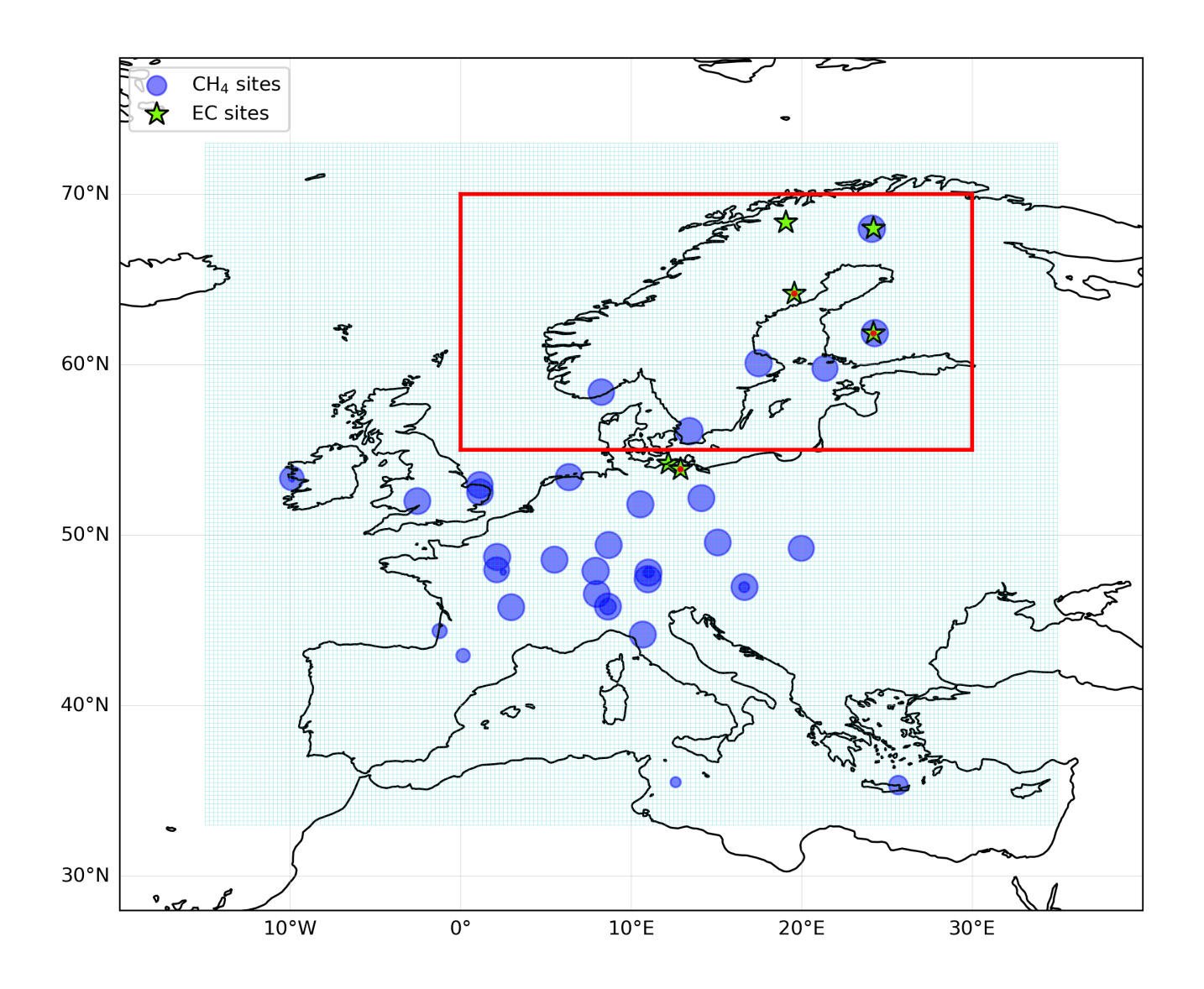


Figure 1. LUMIA inversion domain (cyan grid), the position of the observations used in the LUMIA inversions (blue dots, with the area proportional to the number of assimilated observations); position of the eddy-covariance sites used in the GRaB-AM optimization (green stars) and Nordic domain of interest (red box). The red dots mark the position of the EC sites used in Section 3.3.1 covering the year 2018 (Figure 9) are marked with a red dot.

ing observations over different years within this time period) were assimilated. The number of sites used for the GRaB-AM optimization exceeds the indicated sites shown in Figure 1 (a full list of the sites is given in ?Kallingal et al. (2024b)).

In this study we computed two ensembles of hundred gridded LPJ-GUESS simulations each, randomizing the values of the LPJ-GUESS parameters adjusted by the GRaB-AM algorithm. In the first ensemble (LPJ-GUESS-unopt) the parameter values were drawn based on their prior estimate and standard deviations of 40% of their assumed rangesdraw from a log transform distribution, such that 90% of the prior samples fall within their assumed $\pm 40\%$ uncertainty range. In the second ensemble (LPJ-GUESS-opt), the ensemble members were drawn from the corresponding 90% confidence interval(1.645 time the standard deviations) of the posterior distribution after the burn-in period of the MCMC chain, to maintain consistency.

2.2 Atmospheric inverse modelling

The consistency of CH₄ emission from LPJ-GUESS (LPJ-GUESS-unopt and LPJ-GUESS-opt) with atmospheric CH₄ mixing ratio measurements was tested using the LUMIA inversion framework. The comparison requires using an atmospheric transport model, and accounting for contributions of other methane sources, and from lateral boundary conditions. The model data mismatches then serve to infer a further correction to the emission estimates.

2.2.1 Inversion approach

125

130

135

140

LUMIA Monteil and Scholze (2021) (Monteil and Scholze, 2021) is a regional atmospheric inversion setup developed initially to estimate European CO₂ inversions using in-situ concentration measurements such as those provided by the ICOS network (Monteil et al., 2020; Munassar et al., 2023; Gómez-Ortiz et al., 2023). This study is the first application to a non-CO₂ tracer.

The inversion seeks to determine the set of regional CH₄ emissions that is the most consistent with a dataset of observed in-situ CH₄ mixing ratios. The impact of emissions outside the regional domain is provided through a prescribed background term. The link between emissions and volume mixing ratio given by:

$$\mathbf{y} + \varepsilon_{\mathbf{o}} = \mathbf{H}\mathbf{x} + \mathbf{y}_{bg} + \varepsilon_{\mathbf{m}} \tag{1}$$

with $\bf y$ the observations vector contains observations of the atmospheric CH₄ mixing ratio, and $\bf x$ the control vector contains the variables that we seek to optimise: in our case, the daily CH₄ emissions, grouped in two categories (wetlands and non-wetlands), at a 0.25° resolution over a regional domain ranging from -1515°W, 33°S-N to 35°WE, 73°N (Figure 1). The regional transport operator $\bf H$ contains the sensitivity of the observations $\bf y$ to the (regional) emissions $\bf x$ ($\bf H_{i,j}=\partial \bf y_i/\partial \bf x_j$). The background concentrations ($\bf y_{bg}$) are provided as timeseries of baseline concentrations directly at the observation sites, following the two step approach of Rödenbeck et al. (2009) (see Section 2.2.3). The error terms $\varepsilon_{\bf o}$ and $\varepsilon_{\bf m}$ represent respectively the measurement error and the model error.

The optimal control vector $\hat{\mathbf{x}}$ is given as the one that minimises a cost function $\mathcal{J}(\mathbf{x})$, such that

$$\mathcal{J}(\mathbf{x}) = \frac{1}{2} (\mathbf{x} - \mathbf{x_b})^T \mathbf{B}^{-1} (\mathbf{x} - \mathbf{x_b}) + \frac{1}{2} (\mathbf{H}\mathbf{x} + \mathbf{y}_{bg} - \mathbf{y})^T \mathbf{R}^{-1} (\mathbf{H}\mathbf{x} + \mathbf{y}_{bg} - \mathbf{y})$$
(2)

The first part evaluates the goodness of fit of the estimated control vector \mathbf{x} to its prior estimate $\mathbf{x_b}$, normalised by the prior error-covariance matrix \mathbf{B} , which contains the uncertainty of $\mathbf{x_b}$. The right hand side term evaluates the model fit to the observations \mathbf{y} , normalised by the observation error-covariance matrix \mathbf{R} , which combines the model ($\varepsilon_{\mathbf{m}}$) and measurement ($\varepsilon_{\mathbf{Q}}$) uncertainties (i.e. it is the total uncertainty on the model-data mismatch).

The optimal control vector $\hat{\mathbf{x}}$, which satisfies $\nabla_x \mathcal{J}(\hat{\mathbf{x}}) = 0$, is the set of CH₄ emissions that represents the best compromise between fitting the observations and limiting the departures from the prior estimate (which implicitly carries the knowledge of the models and data used to construct the prior emissions).

The solution is searched for iteratively, using a conjugate gradient algorithm provided by the python "scipy.optimize" package (which employs a nonlinear conjugate gradient algorithm by Polak and Ribiere, a variant of the Fletcher-Reeves method described in (https://docs.scipy.org/doc/scipy/reference/generated/scipy.optimize.minimize.html#rdd2e1855725e-5) pp.120-122). This solver is not optimal for our setup (a linear CG algorithm would be better suited, since our optimization problem is strictly linear), but turned out to be more practical and I/O efficient than the Lanczos (1952) linear solver used in previous LUMIA papers (e.g. Monteil et al. (2020); Munassar et al. (2023)), while giving qualitatively equivalent similar results.

2.2.2 Regional transport model

155

170

180

The regional transport operator **H** was computed using the FLEXPART 10.4 Lagrangian particle dispersion model (Pisso et al., 2019). FLEXPART is not called directly within the inversion, but is used before, to pre-compute observation footprints, i.e. rows of the **H** matrix from Equation 2. These footprints are stored on disk and simply read during the successive phases of the inversion. Each footprint was obtained by simulating the dispersion, backward in time starting from the observation time and position, of ten thousand virtual air particles, based on meteorological fields from the ECMWF ERA5 reanalysis (at a 0.25°, hourly resolution), and limited to the aforementioned European domain: the particles are destroyed when they reach the edge of the domain. The aggregated residence time of the particles near the surface (below 100 m above ground) is used as a proxy for the sensitivity of the observations to the emissions.

175 2.2.3 Boundary conditions

The background vector \mathbf{y}_{bg} accounts for all the contributions to the observed CH_4 mixing ratio that are not adjusted by the inversions: the impact of the initial condition, the impact of CH_4 emissions from outside the regional domain, the impact of European CH_4 emissions having left the domain on the CH_4 mixing ratio of air masses (re-)entering it, and the impact of the various CH_4 sinks (reactions with OH, and, in the stratosphere, with CI and $O(^1D)$.

The background concentrations were taken from the CAMS v19r1 global CH₄ reanalysis of surface observations (Segers, 2020), which relies on the TM5-4DVAR global atmospheric inversion system. The concentrations baselines were extracted using the two-step scheme of Rödenbeck et al. (2009) (see also Bergamaschi et al. (2022) for the CAMS implementation, and Monteil and Scholze (2021) for the usage in LUMIA). These baselines were provided as part of the CoCO2 CH₄ inversion intercomparison, therefore they are purely an external input to our modeling setup.

2.2.4 Prior emissions and uncertainties

185

190

195

215

The inversions solve for CH₄ emissions grouped in two "super-categories": wetland and non-wetlands. The latter groups the contributions of all remaining categories, both anthropogenic (mainly agriculture, waste management and fossil fuel emissions), and natural (geological emissions, termites, lakes and oceans). Anthropogenic emissions are taken from the EDGAR v6.0 emission inventory (Crippa et al., 2019), wetland emissions are taken from the LPJ-GUESS simulations described in Section 2.1.1, with or without the parameters optimization described in Section 2.1.2 (depending on the simulation). Natural emissions are taken from various climatological estimates, reported in Table 1. All the emissions were regridded from their original resolution to the 0.25°, daily resolution of the FLEXPART footprints.

The spatial distribution of the emissions is shown in Figure 3, while their temporal distribution is shown in Figure 2. Wetland emissions are the only category that has exhibits a strong seasonality (biomass burning emissions are seasonal as well, but very low overall, so their influence on the observations contribution to the seasonality of total emissions is negligible). There is also a geographical separation between emissions from wetlands, which are concentrated in Northern Europe, and emissions from the other categories, which are more significant in the rest of the continent, and tend to overlap in time and space. This, and the fact that the observation network is relatively dense in Northern Europe (Figure 1), where wetland emissions are important, justify resolving wetland emissions separately from the other CH₄ sources in the inversions.

The emission uncertainties are stored in the prior error-covariance matrix \mathbf{B} , which is composed, for each category c, of four components: the vector $\sigma_{\mathbf{x}_c}$ containing the standard deviations of the emission themselves, two correlation matrices, C_c^h and C_c^t , storing respectively the prescribed correlations in the spatial and in the temporal dimension, and a scalar scaling factor γ_c , which is used to enforce a specified total annual uncertainty. No cross-category correlations are assumed, therefore the error-covariance matrix is written, for each category, as:

$$\mathbf{B_c} = (C_c^t \otimes C_c^h)^T \sigma_{\mathbf{x_c}}^T \gamma_c^2 \sigma_{\mathbf{x_c}} (C_c^t \otimes C_c^h)$$
(3)

For wetland emissions, the standard deviations $\sigma_{\mathbf{w}}$ are directly given by $\sigma_{\mathbf{x}_c}$ are set to the standard deviation of the LPJ-GUESS ensembles (Sections 2.1.1), whereas for non-wetland emissions, they are set proportional to the absolute value of the emissions. Note that only their relative values matter, since the total uncertainty is determined by γ_c . The inversion-specific values used for γ_c . The scaling factor γ_c is then determined such that $\left(\sum_{ij} \mathbf{B}_c^{ij}\right)^{-1/2}$ equals the desired annual uncertainty for category c. This facilitates comparisons between simulations with different correlation structure, as their overall uncertainty remain identical.

The uncertainties on non-wetland emissions were set to $5 \, {\rm TgCH_4/year} \, (\approx 15\% \, {\rm of} \, {\rm the \, annual \, emissions})$, with C^t and C^h are provided in Section 3.1 constructed as correlation-decay functions $(corr(x) = e^{-x/L})$, with horizontal correlation length of $500 \, {\rm km}$ and temporal correlation length of $30 \, {\rm days}$. For wetlands, the annual uncertainty was set to $0.5 \, {\rm TgCH_4/year}$, with temporal correlation length of $30 \, {\rm days}$. The spatial correlations were either constructed using the same approach, with spatial correlation lengths of $1000 \, {\rm km}$, in the main inversions (LUMIA-Lprior and LUMIA-Lpost), or directly using the error correlation structure from the LPJ-GUESS ensembles (see Section 3.1).

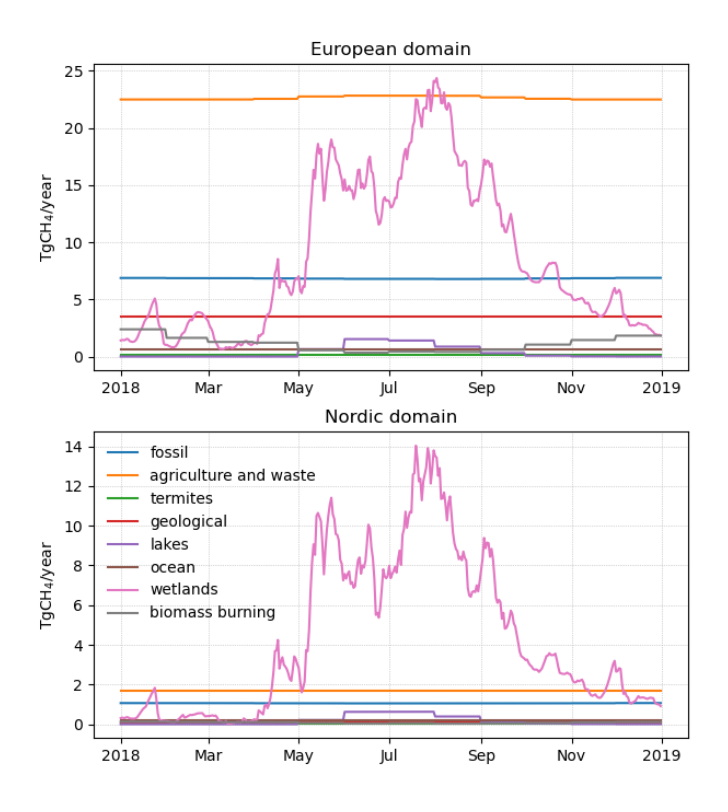


Figure 2. Prior CH₄ emissions used in the "LUMIA-Lprior" inversion.

Table 1. Methane (prior) emissions used in the LUMIA inversions. The spatial resolution reported in the table corresponds to the one as it was made available to us, through the Ioannidis et al. (2025) intercomparison, although the native resolution of some of these products is higher (e.g. EDGAR v6.0 is available at 0.1°)

Category	Annual total (TgCH ₄)	Source	Temporal resolution	ral resolution Spatial resolution	
Wetlands	5.5-8.7	LPJ-GUESS (This study)	daily	0.25°	
Agriculture and waste	22.6	EDGAR v6.0 (Crippa et al., 2019)	monthly	0.25°	
Fossil	6.8	EDGAR v6.0 (Crippa et al., 2019)	monthly	0.25°	
Biomass burning	1.1	GFED-4.1s (Randerson et al., 2017)	monthly	0.25°	
Oceans	0.6	Weber et al. (2019)	monthly	0.25°	yes
Inland water	0.4	Johnson et al. (2022)	monthly	0.1°	yes
Geology	3.5	Etiope et al. (2019)	annual	1°	yes
Termites	0.2	Saunois et al. (2020)	annual	1°	yes

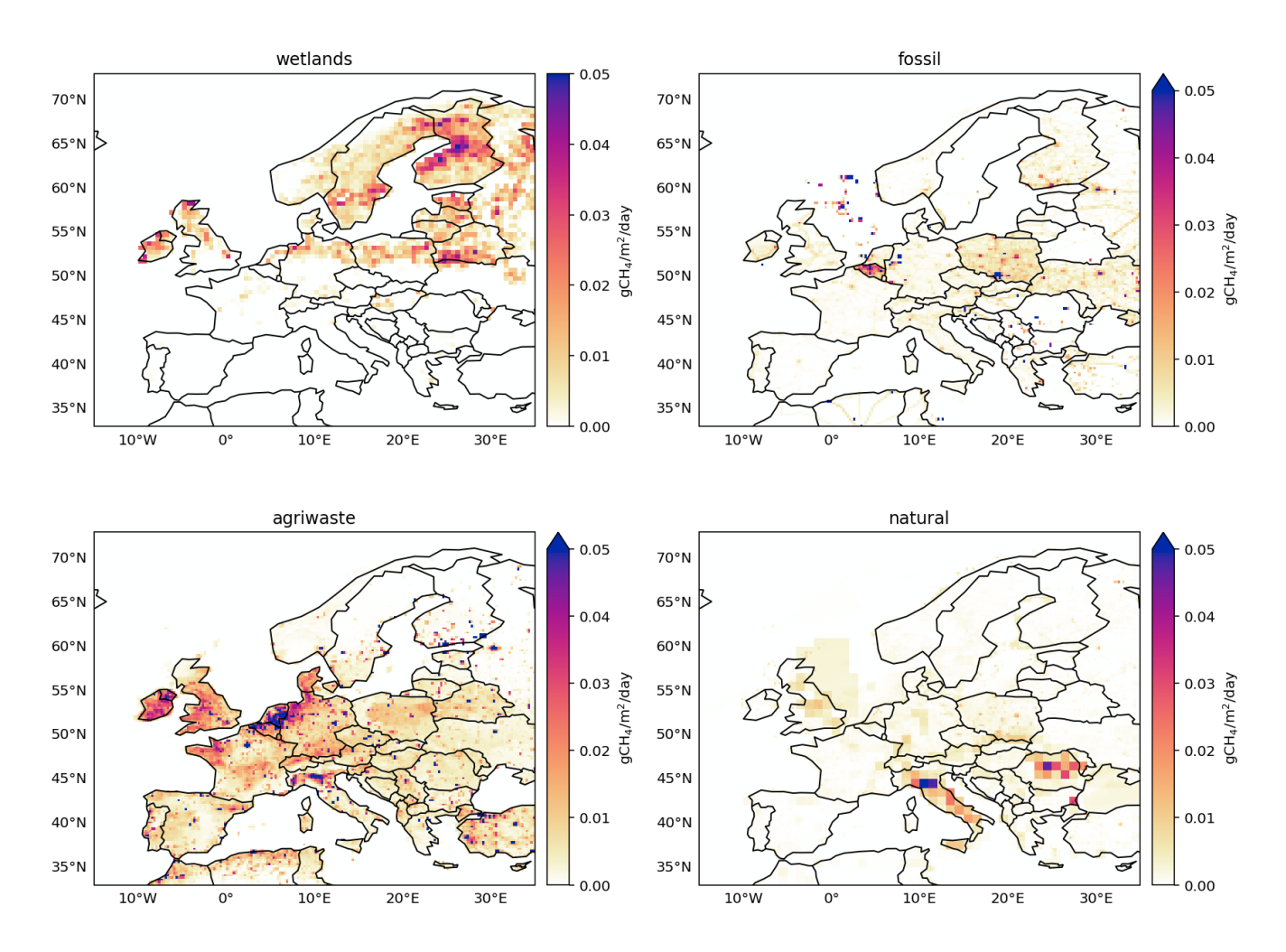


Figure 3. Prior annual average CH₄ emission maps from the natural wetlands, fossil fuels, agriculture and waste and "natural" sectors. The latter groups together emissions from lakes and oceans, geological sources, biomass burning and termites, but is largely dominated by the geological emissions.

2.2.5 Observation and observational uncertainties

220

225

230

235

The LUMIA inversions were constrained by in-situ observations from 43 European in-situ and flask measurement sites, from various observation networks (see Table 2 and Figure 1), most of which are now part of the ICOS network of atmospheric in-situ measurements. The observations were taken from a quality controlled dataset prepared for a CH₄ inverse modeling intercomparison conducted within the CoCO2 project (https://coco2-project.eu/, Joannidis et al. (2025)).

The observation frequency is typically hourly, but we filtered the observations to avoid assimilating observations close to the transition between the planetary boundary layer (PBL) and the free troposphere, as this is where model errors on the PBL height would have the largest impact. For most sites, afternoon data was selected (from 11:00 to 17:00, local time), when the PBL is expected to be the most developed. For high altitude sites (above 1000 m altitude a.m.s.l), night time data was used instead (from 0:00 to 4:00, local time), when the observations are expected to be well above the PBL. At a few sites (Hohenpeissenberg, Hegyhatsal, Ispra, Mace Hear and Pallas), there are also a some observations from flask measurements, for these, no specific filter was applied.

The uncertainties (diagonal of \mathbf{R} in Equation 2) are set as the quadratic sum of the measurement uncertainty ε_{obs} , provided by the atmospheric observations dataset, and of the model uncertainty ε_{mod} . The measurement uncertainty is taken from the observation datasets (when available), with a minimum and default value of 20 ppb. The model uncertainty should in theory be set close to the random component of the error that the model would make when simulating the observations based on the "true" emissions, and excluding systematic component of that error. In practice, that true error is unknown. Here we constructed it as site-specific weekly uncertainty, based on the mismatch between the observed and modelled short term CH_4 variability. The procedure is conducted for each site, in four steps:

- 1. Compute the prior model estimate for the observations, \mathbf{y}_{apri} , corresponding to the prior emissions described in Section 2.2.4.
- Separate the modelled (y_{apri}) and observed (y) time series into baselines and anomalies. The baselines are computed as weekly rolling weighted averages (with the inverse of the measurement uncertainties used as weights), and the anomalies are obtained by subtracting these baselines from their respective timeseries.
 - 3. Compute the standard deviation (σ_{mod}^{site}) of the difference between the anomalies in modelled (prior) and observed CH₄ mixing ratios.
- 4. The model uncertainty of a single observation is finally given by $\varepsilon_{mod}^i = \sigma_{mod}^{site} \times \sqrt{n_{obs}}$, where n_{obs} is the number of observations in a \pm 3.5 days interval surrounding the observation i.

The rationale behind this approach is that the inversions should be able to efficiently reduce the mismatch between the baselines by adjusting the CH₄ emissions, but will likely struggle more with reducing the model-data mismatches between the modelled and observed sub-weekly variability. In practice this results in a larger uncertainty at sites close to large CH₄ emitters, such as Ispra, Saclay and Norunda, reducing their relative weight in the inversion. The last step (4) ensures that the weight of

Table 2. Observation time series assimilated in the LUMIA inversions. The number of observations assimilated is reported in the "nobs" column. Some stations appear twice, when there are both flask and in-situ measurements. The "Model error" column shows the assumed model representation error in the LUMIA-Lprior inversion (the σ_{mod}^{site}). The numbers differ slightly in the LUMIA-Lpost inversion, since they are calculated based on the prior fit to the data). When available, the DOI or PID of the data are shown in their corresponding entry in the bibliography.

Station	Latitude (°N)	Longitude (°W)	Elevation (m a.m.s.l)	Inlet height (m a.g.l)	nobs	Model error (ppm)	Reference
Birkenes, Norway	58.39	8.25	215	3	1937	20.69	Lunder and Platt (2025)
Biscarosse, France	44.38	-1.23	73	47	184	16.57	Lopez and Ramonet (2024)
Mt Cimone, Italy	44.17	10.68	2165	12	2025	25.29	Arduini (2025)
Finokalia, Greece	35.34	25.67	150	15	532	15.02	Delmotte et al. (2024b)
Heidelberg, Germany	49.42	8.68	113	30	2054	33.12	Hammer and Levin (2024)
Hohenpeissenberg, Germany	47.80	11.01	934	131	2105	34.32	Kubistin et al. (2024b)
Hohenpeissenberg, Germany	47.80	11.02	936	5	49	34.32	Lan et al. (2025)
Hyltemossa, Sweden	56.10	13.42	115	150	2162	24.77	Heliasz and Biermann (2024)
Hegyhatsal, Hungary	46.96	16.65	248	96	2056	34.38	Haszpra (2025)
Hegyhatsal, Hungary	46.95	16.65	248	96	47	34.38	Lan et al. (2025)
Ispra, Italy	45.81	8.64	210	16	2316	87.63	Bergamaschi and Manca (2025
Jungfraujoch, Switzerland	46.55	7.98	3570	10	1999	20.26	Steinbacher (2018)
Kasprowy Wierch, Poland	49.23	19.98	1987	2	1783	29.17	Chmura et al. (2024)
Kresin u Pacova, Czech Republic	49.57	15.08	534	250	1995	25.41	Marek et al. (2024)
Lindenberg, Germany	52.17	14.12	73	98	2029	32.56	Kubistin et al. (2024c)
Lampedusa, Italy	35.52	12.62	45	5	47	10.27	Lan et al. (2025)
Lutjewad, Netherlands	53.40	6.35	1	60	2101	91.55	Chen and Scheeren (2024)
Mace Head, Ireland	53.33	-9.90	5	0	1399	9.91	Prinn et al. (2018)
Mace Head, Ireland	53.33	-9.90	5	21	5	9.91	Lan et al. (2025)
Norunda, Sweden	60.09	17.48	46	100	2164	27.16	Lehner and Mölder (2024)
Observatoire pérenne de l'environnement, France	48.56	5.50	390	120	2054	27.47	Ramonet et al. (2024a)
Pallas, Finland	67.97	24.12	560	7	2179	22.33	Laitinen et al. (2025)
Pallas, Finland	67.97	24.12	565	5	32	22.33	Lan et al. (2025)
Pic du Midi, France	42.94	0.14	2877	10	148	12.00	Delmotte et al. (2024a)
Puy de Dome, France	45.77	2.97	1465	10	2009	20.38	Colomb et al. (2024)
Ridge Hill, United Kingdom	52.00	-2.54	204	90	2007	23.62	O'Doherty et al. (2024)
Saclay, France	48.72	2.14	160	100	2100	40.78	Ramonet et al. (2024b)
Hyytiala, Finland	61.85	24.29	181	125	2148	26.98	Levula and Mammarella (2024
Schauinsland, Germany	47.90	7.92	1205	12	2157	23.96	Meinhardt (2025)
Tacolneston Tall Tower, United Kingdom	52.52	1.14	56	185	1939	26.53	O'Doherty and Pitt (2024)
Torfhaus, Germany	51.81	10.54	801	147	2106	26.25	Kubistin et al. (2024a)
Trainou, France	47.96	2.11	131	180	1722	28.69	Ramonet et al. (2024c)
Uto, Baltic Sea	59.78	21.37	8	57	1766	33.33	Hatakka and Laurila (2024)
Weybourne, United Kingdom	52.95	1.12	10	0	1954	32.33	Forster and Manning (2024)
Zugspitze-Schneefernerhaus, Germany	47.42	10.98	2667	3	2142	19.74	Couret and Schmidt (2024)

a site doesn't depend on the observation frequency (if there are more observations within a given week, the individual weight of each observation will be reduced accordingly).

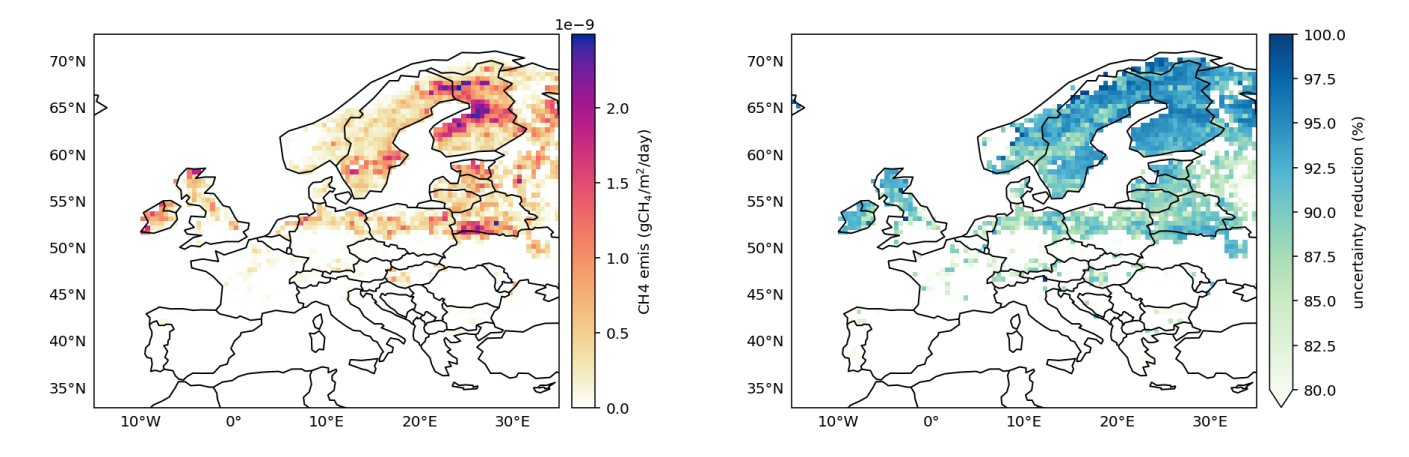


Figure 4. Wetland emission uncertainties, as per the LPJ-GUESS-unopt ensemble (left) and percentage uncertainty reduction in the LPJ-GUESS-opt ensemble (right).

3 Results

255

260

265

270

The LUMIA inversions use wetland emission estimates and uncertainties computed in the two LPJ-GUESS ensembles. We therefore first present the results from these two ensembles, then compare the four CH₄ emission estimates and analyze their consistency with observations.

3.1 Model-derived CH₄-wetland emission uncertainties

The As explained in Section 2.2.4, for each category, the prior error-covariance matrix in LUMIA (B in Equation 2) is constructed, for each emission category, based on three components (see Section 2.2.1): an estimation of the error correlations (in the form of a pair of temporal and spatial correlation matrices), based on a combination of prescribed error correlation structure, a vector of (normalized) prior uncertainties, a total, category-specific and a target annual uncertainty estimate. These settings are typically chosen based on "expert knowledge". However, for the wetland category, the GRaB-AM setup provides an explicit representation of these error correlations.

The emission uncertainties corresponding to the LPJ-GUESS-unopt and LPJ-GUESS-opt simulations were estimated by through two ensemble simulations of 100 members each (see Section 2.1.2). The ensemble standard deviation drops from 6.40 TgCH₄/year in LPJ-GUESS-unopt to 0.45 TgCH₄/year in LPJ-GUESS-opt. In the LPJ-GUESS-unopt ensemble, the uncertainties are concentrated in regions with strong CH₄ emissions: Northern Finland, Scandinavian Arctic, Southern Sweden, Southern Poland and North-West coasts of Ireland and Scotland (Figure 4). The GRaB-AM optimization reduces the uncertainties everywhere, but predominantly at high-latitudes, with the strongest reduction (\approx -95%) being obtained in the Nordic region.

The error correlations are arguably more important for the LUMIA inversions: large error correlations effectively reduce the dimensionality of the problem, making it in turn easier to resolve the contributions from separate categories. Full error covariance matrices can be computed from the ensemble but are too large to fit in memory and be of practical use in the inversions. Instead, in Figure 5, we show the average error correlations as function of distance (in space and time).

The error correlations are generally larger in the prior ensemble (LPJ-GUESS-unopt) than in the posterior one. In the spatial dimension, there is a lot of variability, but overall, there is a very rapid drop in correlation values, which stabilize around 0.55 in LPJ-GUESS-unopt and around 0.35 in LPJ-GUESS-opt, after approximatively 250 km. The correlations decline further with increased distance, but at a very slow pace. Temporally, correlations decrease almost instantly in LPJ-GUESS-unopt, but remain in a 0.55-0.65 range after that, whereas they decrease more gradually in LPJ-GUESS-opt, reaching below 0.4 after 200 days.

The interpretation of spatial correlations is further complexified by the fact that the number of active CH₄ emission grid cells is not constant throughout the year, and therefore the correlation-distance relationship is not constant. For computing Figure 5, we ignored the time dimension for the spatial correlations plot, and the space dimension for the temporal correlation plot (therefore, the averaged correlation for two points distant by e.g. 500 km includes the correlation between emission components at different times of the year). This somewhat mimics the way the prior error-covariance matrix **B** is constructed in LUMIA (i.e. with correlations based on as a Kronecker product of spatial and temporal correlation matrices).

We performed an ensemble of sensitivity tests to determine the most appropriate formulation for the error-covariances in LUMIA. The two main inversions, LUMIA-Lprior and LUMIA-Lpost, use the wetland error distributions ($\sigma_{\mathbf{x}}$ in Equation 3), but correlation matrices based on more traditional exponential correlation-decay functions ($corr(x) = e^{-x/L}$), with correlation lengths L_h of 1000 km in C_h (shown in Figure 5), and $L_t = 30$ days in C_t , and their annual uncertainty $\gamma_{wetland}$ domain-wise annual uncertainty was set to 0.5 TgCH₄/year. This is lower than the variability of the LPJ-GUESS-unopt ensemble, but that variability of that is purposefully unrealistically high to allow GRaB-AM to explore the space of solutions.

In addition, two sensitivity inversions were computed, LUMIA-Lprior+corr and LUMIA-Lpost+corr, which take their annual uncertainty ($\gamma_{wetland}$) directly from the standard deviation of the annual emissions in their corresponding LPJ-GUESS ensemble, and use the ensemble-based correlation-distance relationships shown in Figure 5. The results were very similar in the Nordic region of interest, therefore for most of the analysis, we choose to rely on LUMIA-Lprior and LUMIA-Lpost. This also acknowledges the fact that ensemble-derived uncertainty estimates ignore errors from the driving data of LPJ-GUESS, and from the processes incorrectly modelled in it. Also, the spatial correlations in the ensembles are not constant through time, therefore the decomposition in a spatial and a temporal correlation matrices is not a very accurate approximation of the actual correlations of the ensemble. Finally, setting the annual uncertainty to the same value in both inversion facilitates the interpretation of the results.

3.2 CH₄ emissionemissions

280

285

290

295

300

3.2.1 Annual CH₄ emissions

The non-optimized LPJ-GUESS model (LPJ-GUESS-unopt) points to an emission total of 8.7 TgCH₄/year from natural wetlands, including 4.3 TgCH₄/year in the Nordic sub-domain. The GRaB-AM optimization suggests lowering these values to

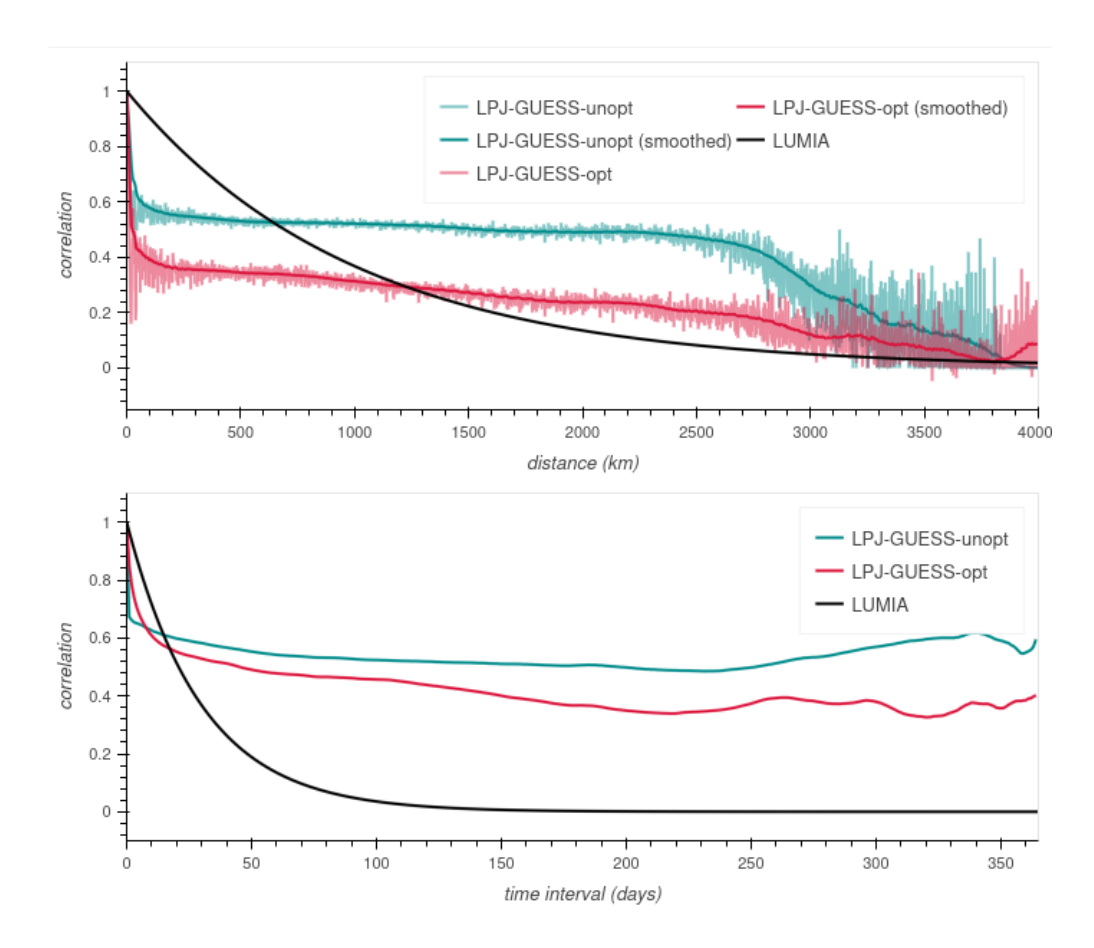


Figure 5. Spatial (top) and temporal (bottom) correlation-distance relationships for the two LPJ-GUESS ensembles. The black line represents the correlation settings used in the LUMIA simulations.

5.5 TgCH₄ (All three observation-informed estimates point to emission reductions ranging from -37%) and 2.5 (LPJ-GUESS-opt, 5.5TgCH₄ (-42%), respectively. The two LUMIA inversions point to further reductions, down to 4.2 TgCH₄/year, including 1.3 TgCH₄ (to -51% (LUMIA-Lpost, 4.3 TgCH₄/yearin the Nordies, in LUMIA-Lprior (respectively -52% and -70% compared to LPJ-GUESS-unopt), and down to 3.0 TgCH₄ at the European scale, and from -42% (LPJ-GUESS-opt, 2.5 TgCH₄/year(-65%) with 1.1 TgCH₄ to -60% (LUMIA-Lpost, 1.7 TgCH₄/year(-74%) in the Nordies, in LUMIA-Lpost (Figure 5 Nordic subdomain
 (Figure 6). The two sensitivity inversions also lead to very similar results (Figure 6 See full results in Table S1).

In contrast, the inversions lead to much lower adjustments to non-wetland emissions, both in relative and absolute terms. The priors (i.e. LPJ-GUESS-unopt and LPJ-GUESS-opt in Figure 6) are 35 TgCH₄ for the full domain, and 35.3-34.3 TgCH₄/year (+0.85-2.8%) and 36-35.2 TgCH₄/year (+2.9-0.1%) respectively in LUMIA-Lprior and LUMIA-Lpost. The contribution of the Nordic region to this is very small, with 3.3 TgCH₄/year in the prior (comparable in magnitude to the wetland emissions in that region). The inversions reduce these to 2.4-2.2 TgCH₄/year (-27-33%) and 2.6-2.5 TgCH₄/year (-21-25%), respectively

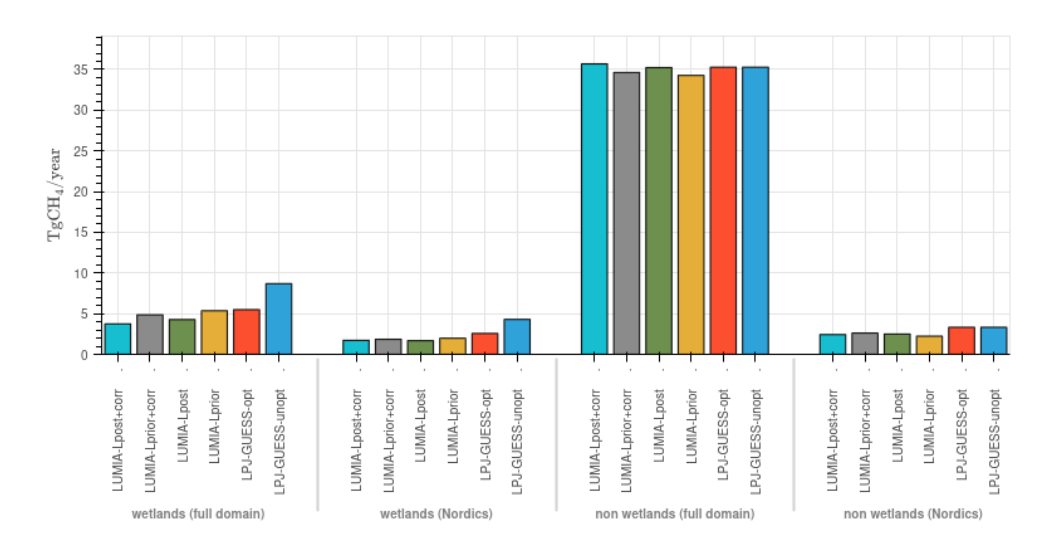


Figure 6. Annual emission estimates (in TgCH₄/year) for the wetland and non-wetland emission categories. LPJ-GUESS-unopt and LPJ-GUESS-opt are respectively the priors of LUMIA-Lprior(+corr) and LUMIA-Lpost(+corr).

in LUMIA-Lprior and LUMIA-Lpost. Here again, the difference between the reference inversions and their sensitivity run counterparts is insignificant very small.

3.2.2 Seasonal cycle of the wetland emissions

325

330

Temporal emission adjustments are shown in Figure 7 (note the different y-ranges in the figure). For the figure clarity, results from the LUMIA-Lprior+corr and LUMIA-Lpost+corr inversions are shown in SI Figure 1Figure S1.

For wetlands, the patterns are very similar between the full-domain and the Nordic region (which reflects the fact that this region accounts for more than half of the European wetland emissions). In LPJ-GUESS-unopt, the emissions remain close to zero in the first quarter of the year, except for two small peaks at the end of January and of March. The emissions then follow a "double-peak" pattern, with a first peak around late mayMay, particularly pronounced in the Nordics, and the main peak in August, after which the emissions decline steadily to reach nearly zero at the end of the year.

The assimilation of in-situ flux data in LPJ-GUESS-opt leads to roughly a halving of the emissions, mainly during the May to October period. Within the Nordic region, the May emission peak emission peak in May is almost fully preserved, whereas the remaining part of the summer variability is smoothed. Outside the Nordics, the temporal structure of the emissions is better preserved. LPJ-GUESS-opt points to a reduction of the amplitude of the emission peaks in January-February (mostly visible outside the Nordics). On the other hand, the emissions after October remain similar to LPJ-GUESS-unopt.

The two main-LUMIA inversions lead to very consistent results within emission reduction in the Nordic region, only with more short-term variability in LUMIA-Lprior that are overall consistent with those obtained in LPJ-GUESS-opt, in particular during the summer months (June-August). Both inversions point to a nearly complete reduction of further attenuate the May emission peak found in the compared to both LPJ-GUESS simulations, and to summer emissions further reduced compared

to LUMIA-Lpost, especially after September estimates, and also point to lower emissions than the LPJ-GUESS simulations after August. LUMIA-Lprior essentially retains the seasonal cycle shape of its prior (LPJ-GUESS-unopt), but with a reduced amplitude, whereas LUMIA-Lpost infers corrections to its prior (LPJ-GUESS-opt) only during some parts of the year (May and August-November).

Outside the Nordics , LUMIA-Lpost (lower left plot in Figure 7), LUMIA-Lprior also leads to a further reduction of the emissions compared to LPJ-GUESS-opt (i.e. its prior) rather annually uniform scaling down of the wetland emissions, compared to its prior (LPJ-GUESS-unopt). LUMIA-Lpost infers almost no adjustment to its prior (LPJ-GUESS-opt) during most of the year, except during June-July where the two simulations are nearly identical. On the other hand, the emissions in LUMIA-Lprior closely follow those in LPJ-GUESS-opt from March to August, which is remarkable because these two emission products have been optimized using two independent techniques, using two completely independent observation datasets last months (October to December), when it leads to a significant (a third to a half) reduction of the baseline emissions, and also completely erases small emission peaks that LPJ-GUESS simulated at the end of October and beginning of December.

The two sensitivity inversions LUMIA-Lprior+corr and LUMIA-Lpost+corr lead to comparable results, on multi-day averages. However, LUMIA-Lprior+corr displays an extremely high short-term variability (much more that LPJ-GUESS-unopt, its prior). We hypothesize that this is due to the very high uncertainty on wetland emissions used in that simulation (6.4 $TgCH_4$, i.e. ≈ 13 times more than in the other inversions), which, associated to the fact that LPJ-GUESS-unopt tends to alternate (at the grid cell level) between days with strong emissions and days with near zero emissions, makes that inversion very underconstrained. However, on a multi-day average, it is remarkably similar to LPJ-GUESS-opt within the Nordic region, until August, and to LUMIA-Lprior for the rest of the year, and also in the rest of Europe. The difference between LUMIA-Lpost and LUMIA-Lpost+corr is mainly in extra-Nordic wetlands, where LUMIA-Lpost

Compared to LUMIA-Lprior, LUMIA-Lprior+corr infers a further reduction of the estimate follows very closely the seasonal variability of their prior (LPJ-GUESS-opt), shifting it only by a seemingly constant scaling factor. This is a consequence of the longer spatial correlations in that inversion very long distance correlations from the LPJ-GUESS ensemble (see Figure 5), which propagate the emission adjustments over larger distances reduces drastically the degrees of freedom of the inversion, even though the observations provide sufficient constraint to resolve finer scale patterns.

360 3.2.3 Temporal variability of the other emissions

340

345

350

355

365

The temporal adjustments of the "non-wetlandemissions" emission category groups contributions from many source processes, mainly anthropogenic, which makes them difficult to interpret at the domain-scale. In the Nordics, the LUMIA inversions infera 11% (LUMIA-Lprior) and 20% (LUMIA-Lpost), on average, a reduction of the non-wetland monthly emissions from January to June. In July both inversions point to a modest increase (+4-7%) compared to the prior, after which the emissions are progressively reduced, emission of 25% (LUMIA-Lpost) to reach 32% (LUMIA-Lprior), with large variations throughout the year, with a peak increase of up to 35% (LUMIA-Lpost, in August), and a reduction to near zero towards the end of the year. This is unrealistic, however the amplitude of

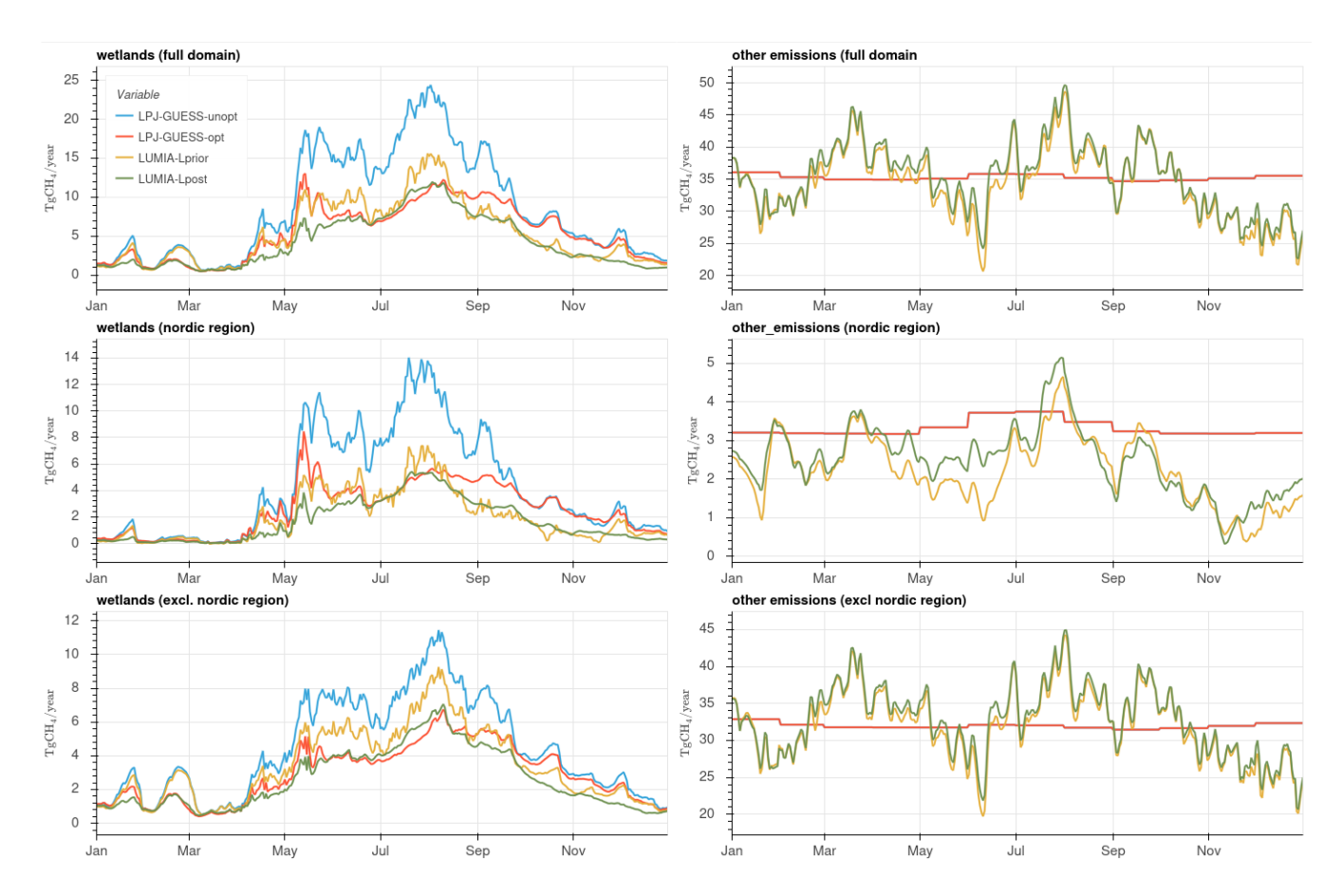


Figure 7. Daily emissions in the entire domain (top), in the Nordic region (middle) and outside it (bottom), for the wetland (left) and non-wetland (right) CH₄ emissions.

A part of this variability is likely caused by misattributions of emission corrections between the two emission categories. For instance, from April to July, the non-wetland emissions of LUMIA-Lprior in the Nordics are significantly lower than those inferred in LUMIA-Lpost, which compensates for an opposite sign difference between these two inversions in the wetland emission category. However, while the reduction in non-wetland emissions reduction is too large to just result from a flux misattribution: if re-attributed towards the end of the year doesn't appear probable given the expected stability of anthropogenic emissions over the year, re-allocating it entirely to the wetland category, this emission category would lead to (significantly) negative wetland emissions—, which isn't realistic either.

370

375

A possible alternative (or complementary) explanation could be error in the CAMS boundary condition: the background concentrations (y_{bg} in Equation 2) explains nearly 100% of the observed mixing ratio on several days towards the end of the year, especially at Hyytiälä (SMR) and Birkenes (BIR). The situation is also similar in the two sensitivity inversions.

3.2.4 Spatial distribution

380

385

390

400

405

The emission adjustments inferred in GRaB-AM and LUMIA optimizations are shown in Figure 8(and SI Figure 2 for the sensitivity runs). To facilitate the comparison, wetland adjustments in LUMIA-Lpost are shown relative to the unoptimized LPJ-GUESS estimate (LPJ-GUESS-unopt). Maps for the sensitivity inversions are can be found in Figure S2, and Figure S3 shows the maps relative to LPJ-GUESS-opt.

The spatial distribution of wetland emission adjustments is very similar in the five data-informed products, and largely proportional to the LPJ-GUESS-unopt emission estimate itself. The long error-correlations imposed on the LUMIA inversions (and intrinsic to the GRaB-AM optimization), combined with the relative concentration of wetland emissions in Northern Europe, ensure a convergence between the localization of flux corrections.

Among the most marked features in the adjustment to the "non-wetland" category, we note a doubling of the emissions in the Bretagne region of France, and in the Northern part of the Netherlands. This could point to underestimated agricultural emissions, which are important in these two regions. Another marked feature is an important ($\approx 80\%$) reduction of the emissions in Northern Italy, which is well correlated with both high natural emissions (mainly geological) and high agricultural emissions.

We, however, need to ascertain a level of care when interpreting these emission adjustments: For instance emissions in the west of the continent can also result from the need to correct an inaccurate boundary condition. There can also be compensating effects between adjustments of emission hotspots, such as the city of Paris or the Po Valley, and their surroundings. These emission corrections should be investigated, but fall outside the scope of our study.

3.3 Fit to observed data

A classical diagnostic in data assimilation is to compare results (optimized emissions or concentrations) to independent measurements. For GRaB-AM, such a validation has been conducted in **Kallingal et al. (2024b). For atmospheric inversions, the comparison is generally made with independent observations of the atmospheric composition, keeping in mind that biases due to the transport model would likely affect similarly the fit to assimilated data and to validation data.

For this study however, most of the available data in the Nordics has been assimilated, either in the LUMIA inversions (for concentration data), or in the GRaB-AM assimilation (for in-situ flux measurements). The aim of the model-data comparisons in this section is therefore not to derive an objective metric of the respective qualities of each emission estimates, but rather to gain insights on the forcings that lead the two optimizations system to adjust the emissions the way they did to these emission adjustments.

3.3.1 Eddy-covariance flux estimations

CH₄ emissions can be estimated locally on wetland scales using flux measurement techniques such as Eddy-covariance measurements, which involve capturing the covariance between the vertical wind speed and the concentration of methane, providing high-resolution data on gas exchange over wetlands. Such observations are for instance provided by the ICOS network in Eu-

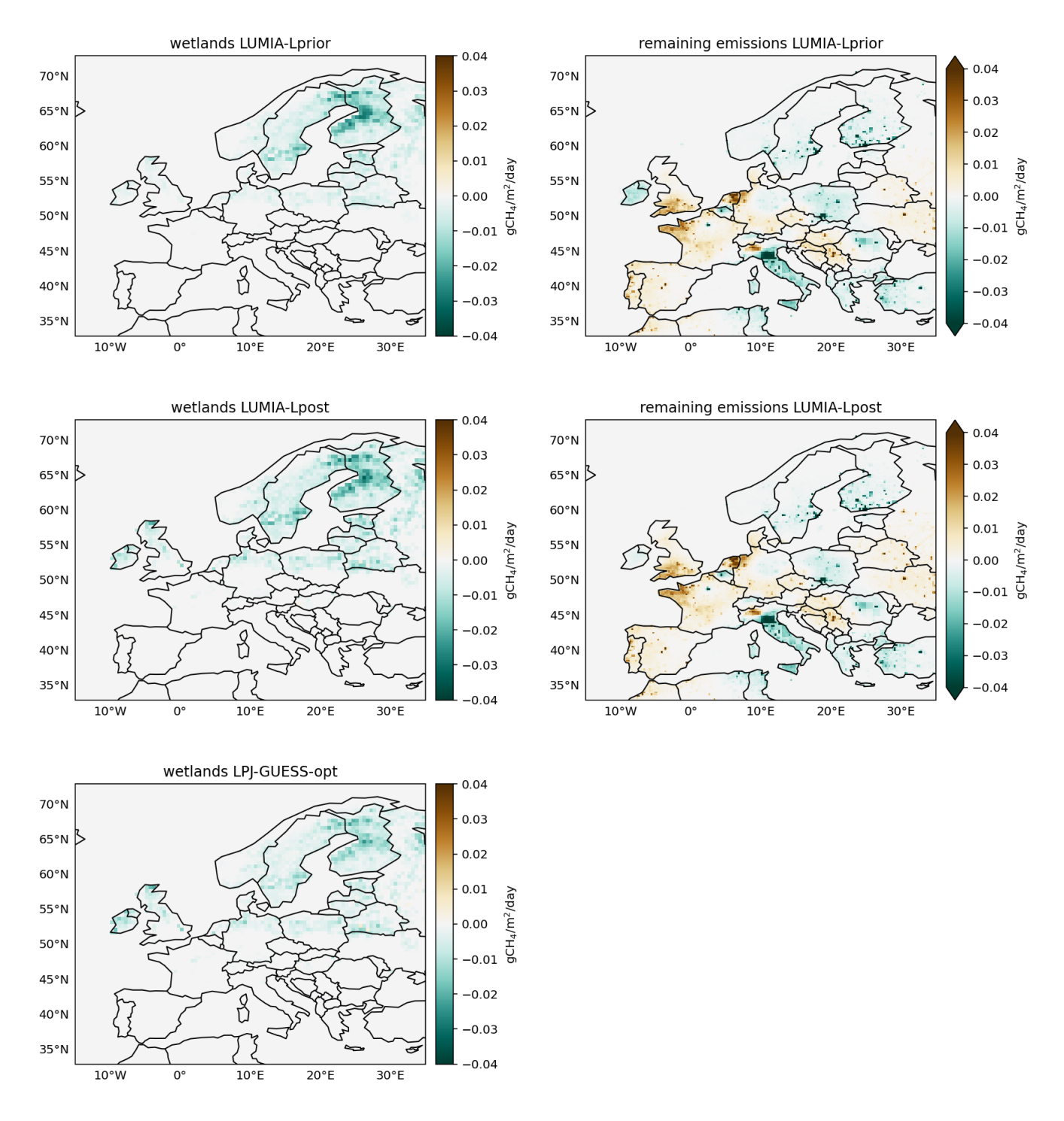


Figure 8. Emission adjustments for wetlands (left) and non-wetlands (right) in the three data-informed simulations, compared to the unoptimized LPJ-GUESS model (LPJ-GUESS-unopt).

Table 3. Mean bias and percentage RMSE reduction, compared to the LPJ-GUESS-unopt site simulation (i.e. negative RMSE reduction values indicate a larger RMSE than the LPJ-GUESS-unopt site simulation), at the three eddy-covariance sites represented in Figure 9.

	RMS	SE reduction	n (%)	Mean bias (gCH ₄ /m ² /day)			
Simulation	Siikaneva	Degero	Zarnekow	Siikaneva	Degero	Zarnekow	
LPJ-GUESS-unopt (site)	-	-	-	0.051	0.028	0.118	
LPJ-GUESS-opt (site)	93 -74 %	98_88_ %	60 % 36 %	0.017	-0.007	-0.016	
LPJ-GUESS-unopt (gridded)	-140 - <u>55</u> %	43-36 %	38 % 23 %	0.085	0.037	0.014	
LPJ-GUESS-opt (gridded)	43-25 %	83 _64_%	4 5 % 26 %	0.038	0.009	-0.027	
LUMIA-Lprior	-3 -10 %	66_56 %	21 % _17 %_	0.022	-0.004	-0.022	
LUMIA-Lpost	93_61_ %	91_76 %	40 % 27 %	0.016	-0.010	-0.037	
LUMIA-Lprior+corr	-20 -21 %	67_57 _%	35 % 17 %	0.031	-0.011	-0.023	
LUMIA-Lpost+corr	77_43 _%	91-72%	30 % 21 %	0.021	-0.005	-0.054	

rope (ICOS RI et al., 2024), and the FLUXNET-CH4 dataset globally (Pastorello et al., 2020; Delwiche et al., 2021), which offers aggregates of high-quality CH₄ fluxes flux measurements from wetlands. These networks try to offer a comprehensive coverage of the different types of wetlands (with differences in physiological features such as hydrology, soil characteristics, vegetation types, etc., and in spatial features, such as geographical distribution, size, landscape position and topography).

However, a direct comparison with gridded emissions is difficult, as the latter accounts for average conditions over the grid cells, which can be very different from the local ones. This is illustrated in Figure 9, which shows a comparison between our four main emission estimates and in-situ flux measurements at three sites in the Nordic region (Zarnekow is slightly outside the Nordic domain used for the emission comparisons, see Figure 1), along with the site-level LPJ-GUESS simulations which were used to train the GRaB-AM optimization (see Section 2.1.2).

The fit of the modelled emissions against the observations is improved for most sites (clearly shown for e.g. Siikaneva and Degero) but since the GRaB-AM optimization is seeking for an optimal parameter set fitting multiple sites simultaneously it is not surprising that there are still larger differences between simulated emissions and observations for any given individual site (as is the case for Zarnekov where the calibrated LPJ-GUESS model fails to simulate the observed peak values during August 2018).

The site-level simulations achieve systematically a better fit to the observations than the their corresponding gridded products. Among the gridded products, the best fit is obtained by LUMIA-Lpost, at Siikaneva and Degero, with RMSE reduction above 9061% (Table 3), whereas the error reduction is lower at Zarnekow, with all the data-informed product in a 40% to 45% error-17% to 21% RMSE reduction range. The two sensitivity inversions using ensemble-derived covariances lead to slightly worse fit than the base LUMIA inversions. We also note a tendency of the LUMIA inversions using LPJ-GUESS-unopt as a prior to infer significant negative emissions on some days (SI figure 4Figure S4): LUMIA adjusts the emissions but preserves most of their original day-to-day variability, which results in days with negative emissions.

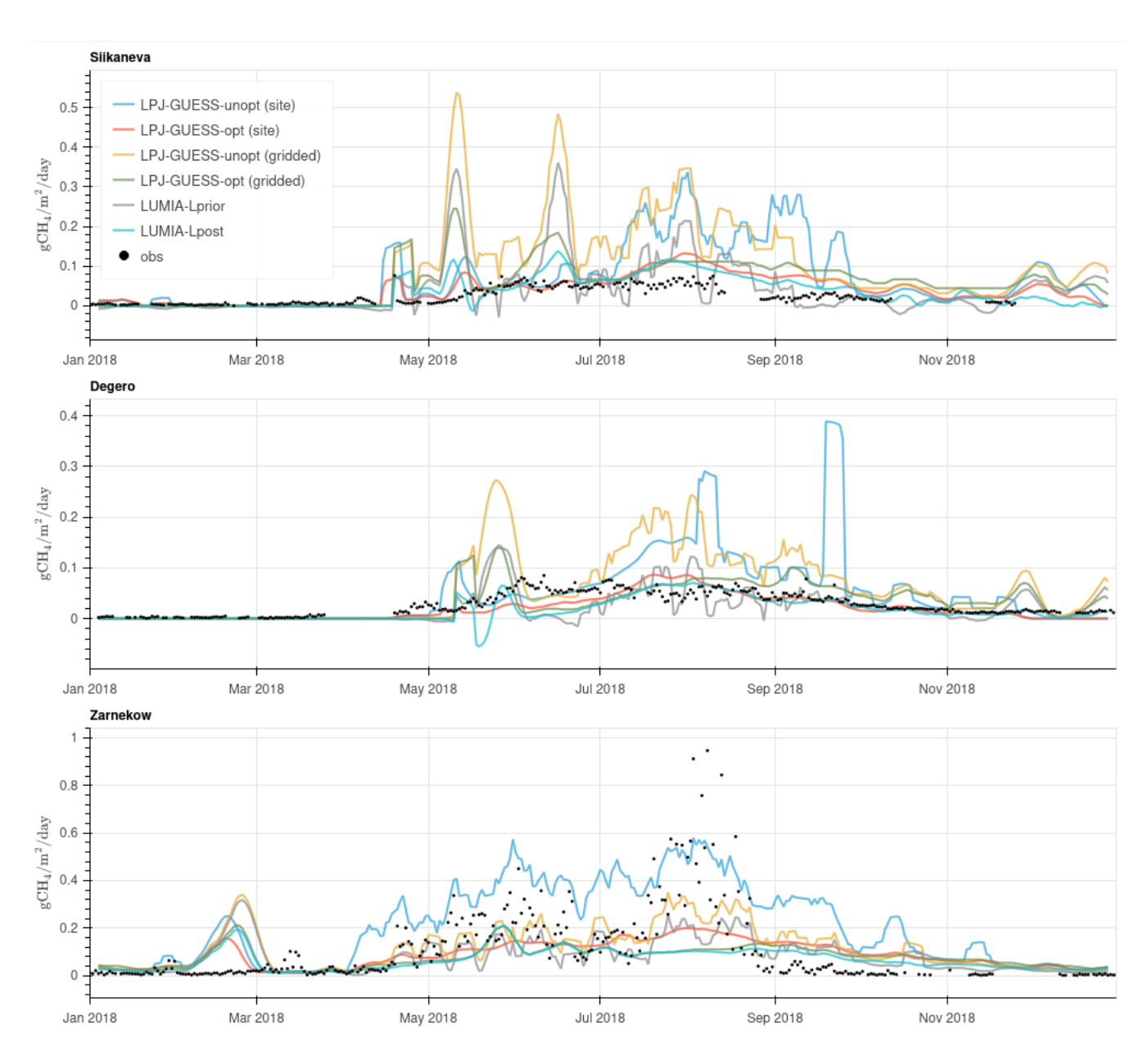


Figure 9. Modelled (solid lines) and observed (dots) methane emissions at three sites within the Nordic region. All the values are expressed in CH₄ emissions per square-meter of wetland. For clarity of the figure, a weekly rolling average has been applied to the modelled data. A version of this figure without smoothing can be found in supplementary materials.

3.3.2 Atmospheric CH₄ observations

The CH₄ concentrations corresponding to the four methane emission estimates are shown in Figure 10, for the six sites in the Nordic region. These sites are also among the ones where the relative contribution of wetland emissions to the foreground concentrations (i.e. the part of the concentrations that can be adjusted by LUMIA) is the highest. For figure clarity, a two-days rolling average has been applied to the the modelled timeseries have been averaged weekly. SI Figures 4 and 5 show, while the data without weekly averaging is shown in Figure S5.

LPJ-GUESS-unopt leads to a strong an overestimation of the concentrations throughout the summer (with a mean bias of up to 40.9-18 ppb at Norunda, and peak model-data mismatches exceeding 300-200 ppb). The fit obtained using LPJ-GUESS-opt emissions is much more in line with the observations, with mean biases ranging from -1.8-2.1 ppb at Hyltemossa to 6.6 ppb at SMR+14.1 ppb at Hyytiälla. However, the CH₄ concentrations are still significantly overestimated during the summer months, in particular at Norunda and Pallastowards the end of the year at Pallas, Norunda and Hytiälla.

The-

435

450

455

460

Both LUMIA inversions lead to very comparable results in terms of mean bias, but with a tendency to underestimate the observations (with biases ranging from -0.5 ppb at Utö, down to -5.4 ppb at Hyltemossa). However, they lead to a significant RMSE reduction compared to the LPJ-GUESS simulations, with RMSE values in a 12.8 ppb to 17 ppb range (slightly lower in LUMIA-Lpostperforms better).

The slightly worse statistics of the LUMIA inversions in terms of RMSE, in particular at Norunda and Pallas (Table 4). At these two sites, the emissions inferred in LUMIA-Lprior lead to modelled CH₄ concentrations bias compared to LPJ-GUESS-opt at the Hyltemossa site (and to a lesser degree also at Birkenes) is likely due to a misfit of observations during the first two weeks of the year, when there is very little flux adjustments that the inversions can infer since the prior emissions start on 1st January. However, the bias is well below the background values on some days. This is a consequence of the negative CH₄ emissions inferred by that inversion, already discussed in Section 3.3.1 typical prescribed model-data mismatches (which are on the order of 30 ppb), and the RMSEs are reduced as expected. Nonetheless, this points to a possible slight underestimation of the emissions by the inversions.

The better fit of the LUMIA inversionsis expected, since they assimilated these data. However,

On the other hand, the overestimation of the observations in the LPJ-GUESS-unopt simulation is very large and a clear indication that the emissions modelled by the non-optimized LPJ-GUESS in the summer are refuted by the atmospheric observations (and to a lesser extent, for the optimized LPJ-GUESS simulation). Other sources of uncertainties (transport model error, uncertainty on the background concentrations, uncertainty in non-wetland emissions) don't seem large enough to account for such an overestimation of the observed data.

4 Discussion

At the global level, methane emissions are relatively well constrained by the observed growth rate of CH₄ background sites, despite uncertainties on the magnitude and trends of the OH sink (Turner et al., 2019). However, significant uncertainties

Table 4. RMSE Fit statistics (bias and RMSE, in ppb) of the LUMIA simulations, for the six sites shown in Figure 10

	Simulation	Hyltemossa	Utö	Pallas	Birkenes	Norunda	Hyytiälla
RMSE	LPJ-GUESS-unopt	26.00- 24.4	39.69 <u>41.1</u>	80.26-45.4	25.50 - <u>22.8</u>	92.95 - <u>38.0</u>	46.97 <u>40.0</u>
	LPJ-GUESS-opt	25.22 <u>24.0</u>	34.44 <u>36.4</u>	39.30-27.0	21.42 <u>21.3</u>	54.10 - <u>32.3</u>	38.21 - <u>37.7</u>
	LUMIA-Lprior	19.23 - <u>17.0</u>	15.76 - <u>15.7</u>	27.63 - <u>17.0</u>	15.92 - <u>15.5</u>	30.52 - <u>14.5</u>	18.06 - <u>15.6</u>
	LUMIA-Lpost	19.13 - <u>17.0</u>	15.32 - <u>15.3</u>	15.90 - <u>12.8</u>	15.57 - <u>15.3</u>	15.64 - <u>13.2</u>	16.17 - <u>15.3</u>
Bias	LPJ-GUESS-unopt	0.8	<u>17.5</u>	18.4	3.3	<u>17.4</u>	<u>19.7</u>
	LPJ-GUESS-opt	-2.1	<u>11.6</u>	6.8	-0.0	<u>11.3</u>	<u>14.1</u>
	LUMIA-Lprior	-5.4	-0.5	-4.0	-3.8	-3.4	-2.5
	LUMIA-Lpost	-5.3	-0.5	-3.8	-3.8	-3.3	-2.6

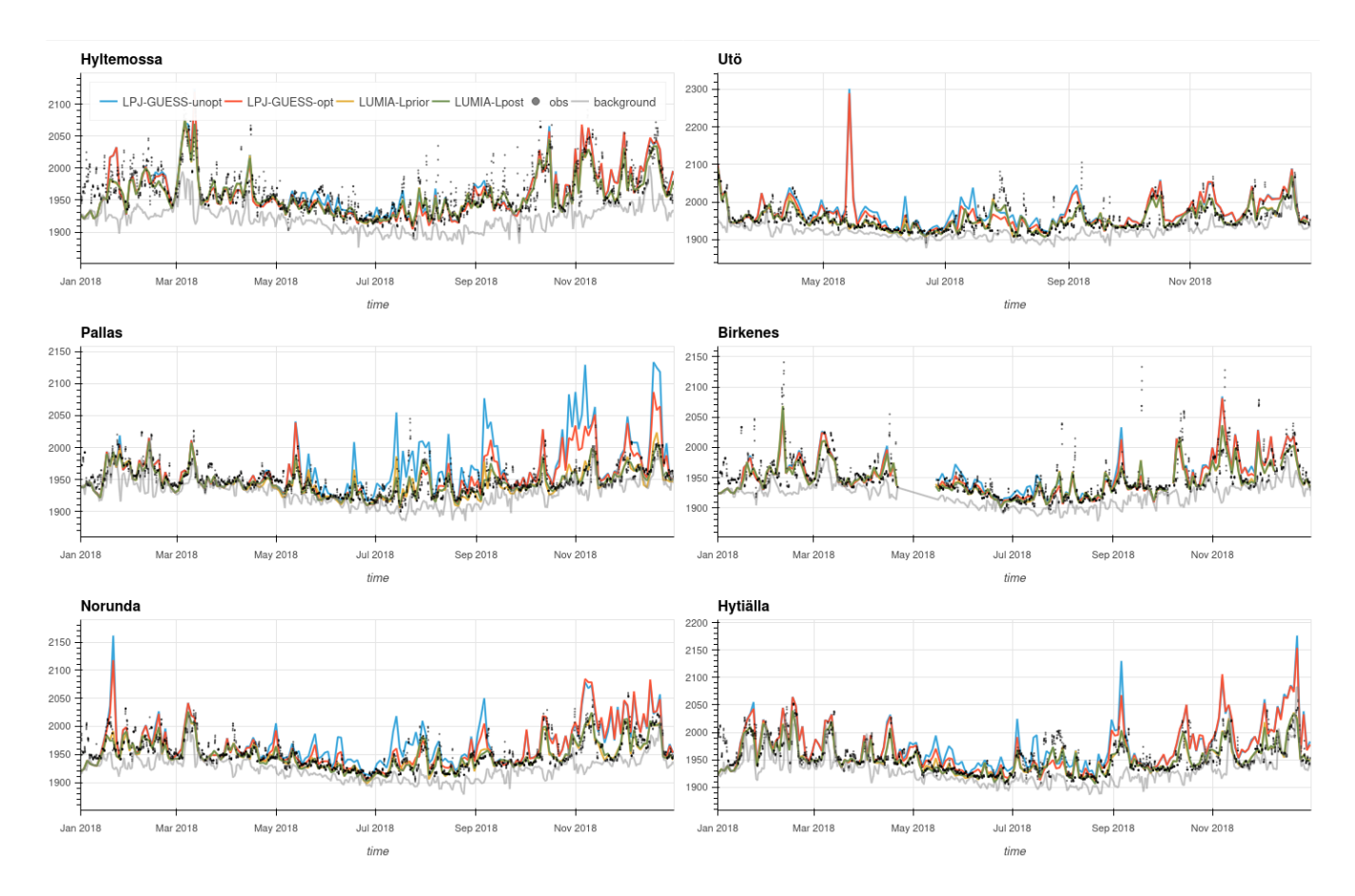


Figure 10. Modelled (solid lines) and observed (dots) CH₄ mixing ratio at the six observation sites within the Nordic region. Modelled time series are shown with as weekly two-days rolling average. A non-smoothed version of the figure can be found in supplementary materials Figure \$5.

remain on regarding both anthropogenic and natural emissions in bottom-up approaches (Saunois et al., 2020). Concerning wetlands emissions specifically, the bottom-up estimates lead to a 40% to 50% uncertainty range (Kirschke et al., 2013; Melton et al., 2013) 465 . Inverse modeling can be used to infer constraints on the emissions at large scales (Bruhwiler et al., 2014; Houweling et al., 2017) , but can only robustly constrain the net methane emissions, since this is what atmospheric CH₄ observations are sensitive to. Satellite observations, such as TROPOMI XCH4 retrievals (Nesser et al., 2024; Tsuruta et al., 2023), or retrievals from the upcoming CO2-M (Sierk et al., 2021) or MERLIN instruments (Ehret et al., 2017), can help increase the resolution at which 470 the emissions are optimized, but their coverage is not constant (cloudiness, short day length at high latitudes in winter, etc.), and their signal-to-noise ratio is lower than that of in-situ observations for detecting emissions (because satellite XCH₄ retrievals quantify the column-averaged CH₄ mixing ratio, therefore they incorporate a stronger background contribution than surface observations). Some implementations of the inverse approach use observations of the isotopic composition of atmospheric methane (δ¹³C-CH₄, δD-CH₄) as a constraint on the source process distribution (Basu et al., 2022; Thanwerdas et al., 2024; Drinkwater et 475 , but the low amount of available data and the uncertainties on the isotopic signatures of methane emissions have limited the practicality of that approach.

Our study combines two data-informed, in principle complementary: the DA, data assimilation approaches: the parameter estimation approach (GRaB-AM) is process-specific and can lead to improvements in the prognostic capabilities of the underlying process model (LPJ-GUESS), but remains subject to possible large scale biases, both because of the lack of representativity of the assimilated data and the inaccuracy of LPJ-GUESS. The inverse approach (LUMIA) s, LUMIA, is arguably more reliable at large scales, but lacks spatial and process resolution.

In this context, the development of a full CH₄ emission data assimilation system (CH4-DAS), combining a vegetation and an atmospheric transport model and capable of assimilating both eddy-covariance measurements and atmospheric CH₄ observations appears as the next logical step. Such systems have been developed successfully for CO₂ (Rayner et al., 2005) and have shown promising results. For methane however, the development is complicated by the need to account for non-wetland methane emissions, which although less uncertain in relative terms, dominate the emission and emission uncertainty budget in absolute terms (Saunois et al., 2020), and by the complexity of wetland models, which can be highly non linear (?) (Kallingal et al., 2024b).

As an intermediate solution, our study explores a two-step approach, with an atmospheric inversion informed by emission estimates and error correlations from a CH₄ DA-parameter estimation approach. In the following sections we further discuss the potential and limitations of both approaches, and how they can help us improve the LPJ-GUESS model.

4.1 LPJ-GUESS parameter estimation (GRaB-AM)

480

485

490

495

The GRaB-AM approach aims at optimizing specifically wetland emissions, by fitting the emissions of a DGVM (LPJ-GUESS) to eddy-covariance (EC) measurements. Indeed, the assimilation of EC yields a clear improvement in the fit not only to ecosystem data, but also to atmospheric CH₄ observations. The resulting emission estimates inherits the spatio-temporal structure from the process parametrizations implemented in the model. This ensures that the emissions remain consistent with their assumed relationships to factors such as climate and environmental forcings. Overall, it should improve the predictive

capacity of the model but can also lead to large systematic errors if the aforementioned parametrizations are insufficiently accurate(such as assumption of zero wind speed above wetlands, the lack of detailed representation of ebullition, and inadequate representation of wintertime emissions in the case of LPJ-GUESS), and/or, if the sites used for training are not representative enough, and/or if the selection of parameters to resolve doesn't provide the necessary degrees of freedom to fit the data. A specific difficulty encountered in GRaB-AM is the high non-linearity of LPJ-GUESS which makes it very challenging to design a minimization algorithm that avoids getting local minima and/or parameter equifinality issues.

The LPJ-GUESS-opt methane emissions used in this study were taken from a multi-site application of the GRaB-AM parameter estimation (Kallingal et al., 2024b). The comparison to atmospheric data however shows that LPJ-GUESS is likely still overestimating CH₄ emissions, even after having assimilated EC measurements. This could be related to the lack of emissions from wet mineral soils in LPJ-GUESS, which hence are attributed to wetlands emissions in this observations and to LUMIA inversion results confirm that, overall, GRaB-AM does lead to an improvement in the quality of the LPJ-GUESS version. The DA (GRaB-AM)improves on this but still results in too high emissions. This essentially points to required CH₄ emission estimate, with annual emission estimates comparable to those obtained through the atmospheric inversions. While this provides a form of validation for GRaB-AM, the comparisons to atmospheric data still shows a tendency to overestimate CH₄ concentrations, in particular in winter (Figure 10). This is also to some extent the case in comparisons with eddy-covariance measurements. This could point to necessary improvements in the model formulation such as for example for the somewhat underlying LPJ-GUESS model; Kallingal et al. (2024b) mentioned in particular the simplistic representation of ebullition and the assumption of zero wind speed above wetlands. Uncertainties in the prescribed wetland area extent could also play a role: the spatial extent of wetlands can vary interannually, depending on hydrological factors such as precipitation, evapotranspiration, and water table depth. However, PEATMAP Xu et al. (2018), which is used in LPJ-GUESS. doesn't capture this variability. Xu et al. (2018) highlights this as a key limitation, noting that the use of static distributions can introduce significant uncertainty, especially in regions with strong seasonal or interannual variability in inundation. Finally, the GRaB-AM optimization did not include a parameter that directly controls the sensitivity of the CH₄ emissions to temperature , following an initial parameter sensitivity analysis conducted on a single-site experiment in Kallingal et al. (2024a). However, our results could indicate an exagerated sensitivity to temperature, as indicated by the persistent emission peak in May, in both the LPJ-GUESS -opt and -unopt ensembles. In this case it would be beneficial to integrate the temperature dependency to the parameter estimation if future applications of GRaB-AM.

4.2 Atmospheric inversion (LUMIA)

500

505

510

520

525

530

This study is the first application of LUMIA inversions to a non- CO_2 tracer. Compared to the latest CO_2 applications Munassar et al. (2023); Gómez-Ortiz et al. (2023), the inversion setup has been simplified: the inversions adjust the emissions directly, instead of offsets to the prior emissions in these studies. This is permitted by the comparatively lower temporal resolution variability of the methane emissions. The uncertainties are of two orders: First, inversions rely on a transport model to establish the link between observed CH_4 mixing ratio and emissions, which can bring systematic errors. Secondly, the source attribution of the emission adjustments depends for a large part of the prescribed emission uncertainties and error correlations.

The original aim was to construct the wetland emission error-covariance matrices based on the variability of the LPJ-GUESS ensembles. However, the ensemble correlations could not be (in a practical manner)approximated and inverted for using in LUMIA (in part because the spatial error of CH₄ emissions. These ensembles contain long distance correlations (see Figure 5), which would theoretically provide constraints to help resolve the relative contribution of wetlands to the total CH₄ emissions. However, this carries the risk of producing biased results if these correlations are not constant through time)accurate, which is likely, given the limitations highlighted in the previous section. We therefore opted for a more conventional approach to constructing the error-covariance matrices in LUMIA-Lpri and LUMIA-Lpost, using the ensemble variability only to distribute a prescribed annual uncertainties in time and space. Results within the Nordic region of interest were very similar to those obtained in the "+corr" sensitivity runs(at least LUMIA-Lpost+corr), which is an indication that, in this region, the observations provide robust enough constraints on the emissions.

The uncertainty associated to transport is difficult to assess independently. Comparisons to independent (i.e. non assimilated) observations rely on the same model to estimate the link between concentrations and emissions, therefore they don't constitute a totally independent validation of the source-concentration relationships themselves. Model intercomparisons, such as TRANSCOM for global models (Gurney et al., 2004), and EUROCOM for regional models (Monteil et al., 2020) can help identifying divergences between models and inversion approaches. A detailed intercomparison was conducted between the LU-MIA and CarboScope-Regional (CSR) inversion systems to quantify the importance of model biases in regional CO₂ inversions (Munassar et al., 2023), which highlighted a stronger sensitivity to emissions in LUMIA. While this could lead to overestimating the methane concentrations (given the correct emissions), the amplitude of the mismatches in LPJ-GUESS-unopt, and the fact that they occur specifically in regions with important wetland emissions rather plead for a significant overestimation of the methane emissions by LPJ-GUESS.

Both inversions pointed to a reduction of non-wetland emissions in the Nordic region suggest an almost complete reduction of non-wetland emissions towards the end of the year , which seems unrealistic: fossil-fuel emissions (which dominate non-wetland emissions in the Nordic region) are not expected to display such intra-annual variability. However, it cannot be entirely a mis-attribution error, since the reduction in , which doesn't seem likely given the importance of fossil-fuel emissions in that non-wetland emissions is an order of magnitude larger than the (posterior) wetland emission themselvesemission category. Comparisons with eddy-covariance data (Figure 9) show an overestimation of emissions from wetlands at Siikaneva and Zarnekow during that period, suggesting possible misattribution of the emission corrections to the non-wetland category. On the other hand, fully re-allocating these corrections to wetlands would imply negative emissions, which is also implausible. We noted that the CAMS background concentrations were very close to (or even occasionally higher than) the observed values in winter, especially at Pallas and Hyytiälä (Figure 10): as widespread negative emissions of CH₄ are unrealistic, this points to an overestimation of the background concentrations by the CAMS concentration baselines. This could lead to a , and a possible widespread bias in the inferred emissions, but emission totals, although it is difficult to determine whether it affects the whole inversion period or just the winter months.

Some inversion systems allow the boundary condition to be adjusted (e.g. Steiner et al. (2024)), but this is risky in the absence of a proper quantification boundary condition uncertainty and of its variability. Here, the non-wetland emission category partly acts as a bias correction, but we must acknowledge this issue as a remaining source of uncertainty.

4.3 Refined estimate of European methane emissions at high latitude

We have refined the wetland emission estimate in the Nordic region to a range of 1.1-1.7 TgCH₄/year (LUMIA-Lpost) to 2.5 TgCH₄/year (LPJ-GUESS-opt), significantly down from 4.3 TgCH₄/year in the original LPJ-GUESS-unopt estimate. While the difference between the LPJ-GUESS-unopt and the other estimates is large, the relative qualities of the three data-informed products are more difficult to assess.

The inversions lead to an improved representation of atmospheric observations, while not significantly degrading compared to LPJ-GUESS-opt, and LUMIA-Lpost also yields a slight improvement in the fit to EC datacompared to eddy covariance data, compared to the gridded LPJ-GUESS-opt. Furthermore, we can speculate that a portion of the flux corrections to Nordie non-wetland emissions inferred by the inversions should in fact be attributed to wetlands: the comparison with in-situ flux measurements shows a tendency of LPJ-GUESS to model emissions in winter which are not confirmed by observations. Emission peaks are modelled in December at Siikaneva and Degero, and in March at Zarnekow (and are likely much more widespread since they are visible in the domain-aggregated emission timeseries shown in Figure 7), but are not present in the EC data. The inversions correct these peaks, but in part through an adjustment of the non-wetland emissions. On the other hand, the potential issues with the background concentrations, highlighted in product. The better fit to the previous section, could indicate an underestimation of the emissions in our inversions, eddy-covariance data by the site-specific LPJ-GUESS simulations (Figure 9) is expected since 1) GRaB-AM has already maximized the fit to these data, leaving only limited scope for improvement to LUMIA, and 2) these simulations use site-specific meteorological forcings, whereas the emissions in LUMIA and in the gridded LPJ-GUESS simulations are representative of larger 0.25° × 0.25° grid cells. Nonetheless, the estimates in LUMIA could also be impacted by systematic error, such as biases from the boundary condition, transport model errors (as highlighted in Munassar et al. (2023)), or category attribution errors, as discussed in the previous sections.

Wetland-Direct comparisons with other studies are complicated because of the small size of our Nordic domain, and other vegetation models have their own shortcomings, and are therefore not necessarily more realistic than LPJ-GUESS. Nonetheless, in a comparison of Arctic wetland emission estimates from Arctic wetlands derived from six different vegetation models were compared in Aalto et al. (2024). They found that, Aalto et al. (2024) found that, although not a complete outlier, LPJ-GUESS was to be clearly at the high end of the rangebut not a complete outlier. Our inversion-optimized estimates, on the other hand, are well in line with the average of that ensemble. In ?, the GRaB-AM optimization adjusted emissions from wetlands located above 45 degrees latitude from 43.09 TgCH. In the Ioannidis et al. (2025) European CH₄ /year to 37.54 inversion intercomparison, in the framework of which our LUMIA CH₄ setup was developed, the JSBACH-HIMMELI model () was used to provide prior wetland emissions. For the same Arctic domain, the annual wetland emissions add up to 1.3 TgCH₄/year. While the inversion part of the study concerns only a small portion of that domain, the reasonable agreement between LPJ-GUESS-opt and the LUMIA inversions reinforces our confidence in the GRaB-AM results.

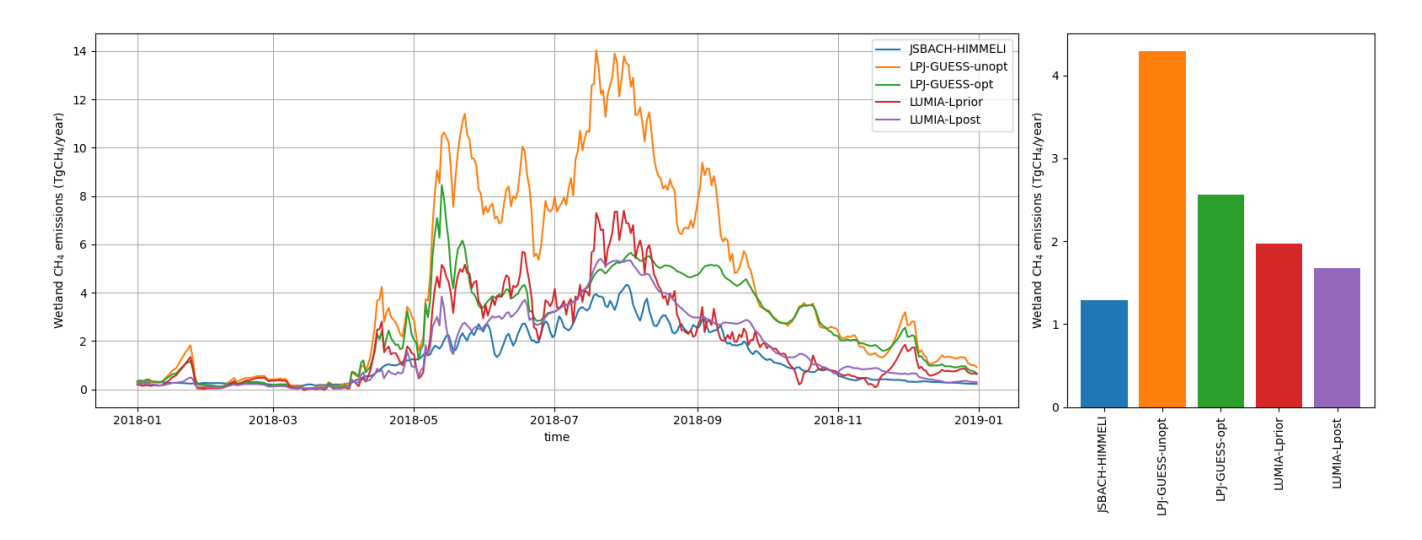


Figure 11. Wetland CH₄ emissions in the LPJ-GUESS and LUMIA products, compared to the JSBACH-HIMMELI emission estimate from Ioannidis et al. (2025).

, 23% lower than the ones in LUMIA-Lpost (Figure 11). LUMIA-Lpost is also the closest to JSBACH-HIMMELI in terms of seasonality, with a summer maximum in August, and near zero emissions in winter time.

Taken together, these comparisons would point at LUMIA-Lpost being the most realistic of our three wetland emission estimates. The contribution of wetlands from our Nordic domain to the overall wetland CH₄ emission budget is however very small, but it suggests a benefit of repeating the study, with an improved setup, over a wider pan-Arctic region.

4.4 Towards a coupled flux-concentration CH₄ data assimilation system

600

615

The initial aim of the study was the implementation of a two-step estimation approach, with a transmission of uncertainty between the flux DA vegetation model parameter estimation (GRaB-AM) and the atmospheric inversion (LUMIA)parts. Two main complications were encountered: first, the error structure from the DA parameter estimation step could not be easily approximated in a form usable by the inversion (i.e. as a set of standard deviations and spatial and temporal correlation matrices). This purely technical limitations could be overcome, e.g. by using an ensemble minimization approach in LUMIA, which usually don't need an explicit representation of the error covariance matrices (e.g. Bisht et al. (2023)).

A more fundamental issue is the complexity of the LPJ-GUESS model (and of dynamic global vegetation models in general), which makes their optimization against eddy-covariance data arduous. The heavy parametrization, non linear interactions, and tightly coupled processes (e.g. Famiglietti et al. (2021)). This could be overcome by the photosynthesis, allocation, soil moisture, plant types, etc.) in the model make its calibration against EC data computationally demanding and prone to equifinality. However, increased complexity doesn't necessarily translate in higher predictive performance (Famiglietti et al., 2021). The development of diagnostic models for wetland methane emissions, e.g. McNicol et al. (2023); Bernard et al. (2025), similar to those existing for CO₂ (Mahadevan et al., 2008; Knorr and Heimann, 1995; Potter et al., 1993), could help overcome these

limitations. In contrast to DGVMs, diagnostic models do not attempt to simulate ecosystems, but focus solely on empirical parameterizing of their emissions based on a handful of known or observable or externally modelled parameters (e.g. net primary production, water table depth, temperature, etc.). Alternative diagnostic models based on Machine Learning (ML) algorithms remove the need to explicitly formulate relationships between the observables and the inferred CH_4 emissions (e.g. Virkkala et al. (2025); Ying et al. (2025); Ross et al. (2024)). This however limits their scope to studying emissions during the observable period (i.e. the past few decades at most), and DGVMs will remain needed for their long-term predictive capabilities, therefore it is crucial to ensure that data assimilation experiments such as ours eventually lead to improvements in the DGVMs.

In the past years, subsequent work has also been conducted by the anthropogenic emission inventory compilers to produce uncertainty estimates (e.g. Solazzo et al. (2021)), which should lead to a better representation of the anthropogenic emission uncertainties in inversions, and in turn improve the reliability of their source attribution.

5 Conclusions

620

625

640

645

We have implemented performed European CH₄ inversions using the LUMIA inversion system, making use of wetland emission estimates and associated uncertainties from a CH₄ emission data assimilation (DA)system (GRaB-AM), based on the regional atmospheric inversion system. Prior estimates for methane emissions from wetlands, as well as the associated uncertainties, were taken from a parameter estimation of the LPJ-GUESS model?. We focused model (GRaB-AM, Kallingal et al. (2024b)), while prior emissions from other methane sources were taken from conventional emission inventories (e.g. EDGAR 6.0 for anthropogenic emissions). The primary objective was to compare and cross-validate the two optimization approaches, but we also wanted to determine whether the additional constraints from eddy-covariance data could help the inversion resolve not only the total CH₄ emissions, but also the contribution from wetlands to this total.

We focused most of our analysis on the estimation of wetland emissions emissions from wetlands in the Nordic region, since wetlands emissions are the most uncertain term in the methane budget, and since they (0°E, 55°N; 30°E, 70°N), where wetlands dominate the emission budgetin that region.

We compared several: this limits the risk that the inversions incorrectly allocate emission adjustments between the wetland and non-wetland categories. We found a strong agreement between the different data-informed wetland-emission estimates: DA of eddy-covariance flux measurements approaches (GRaB-AM), inversion constrained, informed by EC data; LUMIA, informed by atmospheric CH₄ observations (LUMIA), and inversion constrained by atmospheric observations, and, indirectly, by eddy-covariance data (through the EC data informed GRaB-AM prior). All simulations clearly measurements; and LUMIA constrained by wetland emissions from GRaB-AM, informed by both observation types): all three approaches point to a strong (by a factor 2 to 3 two to three) overestimation of the CH₄ wetland emissions by the un-optimized LPJ-GUESS model. The GRaB-AM approach leads to significant improvement of the fit to atmospheric data (which it didn't assimilate), which constitutes a form of additional validation for the approach. The inversion using emissions from the prior wetland emissions from GRaB-AM data assimilation as a prior also leads also lead to the best overall fit to observations.

650 We have explored using model-based error covariances in implementing a more complete uncertainty transmission between the parameter estimation and atmospheric inversion steps, constraining the LUMIA inversions, to improve their capacity to resolve contributions of wetlands to the total methane emissions. The impact was relatively negligible within the Nordic region, but more significant in regions where wetlands with error correlations from the GRaB-AM LPJ-GUESS ensembles. In theory, the long distance correlations in these ensembles should let us extend our analysis to regions where wetland emissions 655 are significant but contribute a smaller fraction of the uncertainty. Making full use of these model-based error covariance would require adaptations in the inversion approach (by e.g. using an ensemble-based optimization technique). It also implies relying on the specific wetlands CH₁ emissions processes as implemented in the emission total. However, despite an improved agreement to atmospheric observations, the fit of LPJ-GUESS DGVM. Nonetheless, these obstacles could be overcome, and our study shows the potential for a joint flux-concentration CH₄ data assimilation system, which we will explore in future studies to eddy covariance data remains sub-optimal, even after the GRaB-AM parameter estimation, suggesting that these 660 error correlations may not be entirely realistic. This points either to shortcomings in LPJ-GUESS itself, or to the need to include more degrees of freedom in the GRaB-AM approach, by increasing the number of parameters, to allow a more realistic fit to the eddy-covariance data in multi-site experiments.

Code and data availability. The source code for this project, as well as a selection of the data (fit to observations, monthly prior and posterioremissions) will be made available on a public repository once the study is accepted. The full datasets and code can be obtained by contacting the main author.

Competing interests. The contact author has declared that none of the authors has any competing interests

675

Author contributions. GM designed the LUMIA inversion system and performed the atmospheric inversions. JTK designed the GRaB-AM data assimilation system and computed the LPJ-GUESS ensembles. GM, MS and JTK collectively designed the study. GM wrote the manuscript, with contributions and critical feedbacks from MS and JTK.

Acknowledgements. We thank Sander Houweling and Liesbeth Florentie for coordinating the inverse modeling intercomparison that lead to this study, preparing and distributing the inversion inputs (prior emissions, observations, background concentrations). We also thank Arjo Segers (TNO) who computed the CAMS simulation and the baseline concentrations used in the inversions. We acknowledge all the data providers cited in Table 2.

We acknowledge the PIs of the in situ flux measurements obtained from FLUXNET (https://fluxnet.org/data/fluxnet2015-dataset/) and AVAA-SMEAR (https://smear.avaa.csc.fi/, for SMEAR II data, Ivan Mammarella and colleagues) for the open data.

We also thank the data providers for the atmospheric observations: Marc Delomotte, Morgan Lopez, Olivier Laurent, Camille Yver and Michel Ramonet from the Laboratoire des Sciences du Climat et de l'Environnement, Sebastien Conil from ANDRA, Francois Gheusi from the Laboratoire d'Aérologie, Aurélie Colomb and Jean-March Pichon from Université Clermont Auvergne, Tobias Kneuer, Dagmar Kubistin, Christian Plass-Duelmer, Matthias Lindauer and Jennifer Mueller-Williams from the Deutscher Wetterdienst, Michael Heliasz, Tobias Biermann, Irene Lehner and Meelis Molder from Lund University, Giovanni Manca from the Joint Research Centre Ispra, Lukasz Chmura and Jaroslaw Necki from the Akademia Górniczo-Hutnicza, Huilin Chen and Bert Scheeren from the University of Groningen, Juha Hatakka and Tuomas Laurila from the Finish Meteorological Institute, Ivan Mammarella from Helsinki University, Jgor Arduini and Stefano Amendola from the University of Urbino, Dep. of Pure and Applied Sciences (DISPEA), Italian Air Force Meteorological Service, Lazlo Haspra from the Hungarian Meteorological Service (now at ATOMKI), Samual Hammer from the Institut für Umweltphysik, Martin Steinbacher from the Swiss Federal Laboratories for Materials Science and Technology (EMPA), Frank Meinhardt and Cedric Couret from the German Environmental Agency (UBA), Kieran Stanley, Simon O'Doherty and Joseph Pitt from the University of Bristol, Martina Schmidt from the University of Heidelberg, and Grant Foster from the University of East Anglia.

This research has been partly supported by the Strategic Research Area "Biodiversity and Ecosystem services in a Changing Climate" (BECC), Lund University (grant no. DnrV 2018/467), and is a contribution to the Strategic Research Area "ModElling the Regional and Global Earth system" (MERGE). BECC and MERGE are funded by the Swedish government. This research has also been partly supported by the "CoCO2" (grant no. 958927) and the "AVENGERS" (grant no. 101081322s) projects from the European Union's Horizon 2020 and Horizon Europe Framework Programmes for Research and Innovation, funded by the European Union.

The computations and data handling were enabled by resources provided by the National Academic Infrastructure for Supercomputing in Sweden (NAISS), partially funded by the Swedish Research Council through grant agreement no. 2022-06725.

References

705

720

- Aalto, T., Tsuruta, A., Mäkelä, J., Mueller, J., Tenkanen, M., Burke, E., Chadburn, S., Gao, Y., Mannisenaho, V., Kleinen, T., Lee, H., Leppänen, A., Markkanen, T., Materia, S., Miller, P., Peano, D., Peltola, O., Poulter, B., Raivonen, M., Saunois, M., Wårlind, D., and Zaehle, S.: Air Temperature and Precipitation Constraining the Modelled Wetland Methane Emissions in a Boreal Region in Northern Europe, EGUsphere, pp. 1–31, https://doi.org/10.5194/egusphere-2023-2873, 2024.
 - Arduini, J.: Atmospheric CH4 at Monte Cimone by University of Urbino, Dep. of Pure and Applied Sciences (DISPEA), https://doi.org/https://gaw.kishou.go.jp/search/file/0074-6042-1002-01-01-9999, 2025.
 - Basu, S., Lan, X., Dlugokencky, E., Michel, S., Schwietzke, S., Miller, J. B., Bruhwiler, L., Oh, Y., Tans, P. P., Apadula, F., Gatti, L. V., Jordan, A., Necki, J., Sasakawa, M., Morimoto, S., Di Iorio, T., Lee, H., Arduini, J., and Manca, G.: Estimating Emissions of Methane Consistent with Atmospheric Measurements of Methane and δ^{13} C of Methane, Atmospheric Chemistry and Physics, 22, 15 351–15 377,
 - Batjes, N. H.: ISRIC-WISE Global Data Set of Derived Soil Properties on a 0.5 by 0.5 Degree Grid (Ver. 3.0), ISRIC Report, 2005, 2005.
 - Bergamaschi, P. and Manca, G.: ICOS ATC CH4 Release from Ispra (100.0 m), 2017-12-15–2025-03-31, https://hdl.handle.net/11676/8yimXenpgumK1-E-AZudMxr1, 2025.
- Bergamaschi, P., Segers, A., Brunner, D., Haussaire, J.-M., Henne, S., Ramonet, M., Arnold, T., Biermann, T., Chen, H., Conil, S., Delmotte, M., Forster, G., Frumau, A., Kubistin, D., Lan, X., Leuenberger, M., Lindauer, M., Lopez, M., Manca, G., Müller-Williams, J., O'Doherty, S., Scheeren, B., Steinbacher, M., Trisolino, P., Vítková, G., and Yver Kwok, C.: High-Resolution Inverse Modelling of European CH4 Emissions Using the Novel FLEXPART-COSMO TM5 4DVAR Inverse Modelling System, Atmospheric Chemistry and Physics, 22, 13 243–13 268, https://doi.org/10.5194/acp-22-13243-2022, 2022.
- Parand, J., Salmon, E., Saunois, M., Peng, S., Serrano-Ortiz, P., Berchet, A., Gnanamoorthy, P., Jansen, J., and Ciais, P.: Satellite-based modeling of wetland methane emissions on a global scale (SatWetCH4 1.0), Geoscientific Model Development, 18, 863–883, https://doi.org/10.5194/gmd-18-863-2025, publisher: Copernicus GmbH, 2025.
 - Bisht, J. S. H., Patra, P. K., Takigawa, M., Sekiya, T., Kanaya, Y., Saitoh, N., and Miyazaki, K.: Estimation of CH₄ Emission Based on an Advanced 4D-LETKF Assimilation System, Geoscientific Model Development, 16, 1823–1838, https://doi.org/10.5194/gmd-16-1823-2023, 2023.
 - Bruhwiler, L., Dlugokencky, E., Masarie, K., Ishizawa, M., Andrews, A., Miller, J., Sweeney, C., Tans, P., and Worthy, D.: CarbonTracker-CH<Sub>4</Sub>: An Assimilation System for Estimating Emissions of Atmospheric Methane, Atmospheric Chemistry and Physics, 14, 8269–8293, https://doi.org/10.5194/acp-14-8269-2014, 2014.
- Chen, H. and Scheeren, B.: Atmospheric CH4 Product, Lutjewad (60.0 m), 2006-05-17–2024-03-31, https://doi.org/https://hdl.handle.net/11676/dvsu8Y6AX9-YmpPwzp-hXVKC, 2024.
 - Chmura, L., Chmura, Ł., and Nęcki, J.: Atmospheric CH4 Product, Kasprowy Wierch (7.0 m), 1996-07-05-2024-03-31, https://doi.org/https://hdl.handle.net/11676/Qowtphdwpy95uFVvqPk-VES_, 2024.
 - Christensen, T. R.: Wetland Emissions on the Rise, Nature Climate Change, 14, 210–211, https://doi.org/10.1038/s41558-024-01938-y, 2024.
- Colomb, A., Ramonet, M., Yver-Kwok, C., Delmotte, M., Lopez, M., and Pichon, J.-M.: Atmospheric CH4 product, puy de dôme (10.0 m), 2011-04-18–2024-03-31, https://doi.org/https://hdl.handle.net/11676/_UMq711VgOR4-5RawhPQC1nU, tex.pid:

https://doi.org/10.5194/acp-22-15351-2022, 2022.

- Couret, C. and Schmidt, M.: Atmospheric CH4 Product, Zugspitze (3.0 m), 2002-01-01-2024-03-31, https://doi.org/https://hdl.handle.net/11676/eFh1N9EGf7oYXbfrwt1IURYw, 2024.
- Crippa, M., Oreggioni, G., Guizzardi, D., Muntean, M., Schaaf, E., Lo, V. E., Solazzo, E., Monforti-Ferrario, F., Olivier, J., and Vignati, E.: Fossil CO2 and GHG Emissions of All World Countries, https://publications.jrc.ec.europa.eu/repository/handle/JRC117610, https://doi.org/10.2760/687800, 2019.
 - Delmotte, M., Gheusi, F., Lopez, M., and Ramonet, M.: Atmospheric CH4 Product, Pic Du Midi (28.0 m), 2014-05-07–2024-03-31, https://doi.org/https://hdl.handle.net/11676/OK113K5n2itBpxIqzgakrZKp, 2024a.
- Delmotte, M., Lopez, M., and Ramonet, M.: Atmospheric CH4 Product, Finokalia (15.0 m), 2014-06-05-2024-03-31, https://doi.org/https://hdl.handle.net/11676/C06b8z3xyRgR4BvFHr4LcxAI, 2024b.
 - Delwiche, K. B., Knox, S. H., Malhotra, A., Fluet-Chouinard, E., McNicol, G., Feron, S., Ouyang, Z., Papale, D., Trotta, C., Canfora, E., Cheah, Y.-W., Christianson, D., Alberto, Ma. C. R., Alekseychik, P., Aurela, M., Baldocchi, D., Bansal, S., Billesbach, D. P., Bohrer, G., Bracho, R., Buchmann, N., Campbell, D. I., Celis, G., Chen, J., Chen, W., Chu, H., Dalmagro, H. J., Dengel, S., Desai, A. R., Detto, M., Dolman, H., Eichelmann, E., Euskirchen, E., Famulari, D., Fuchs, K., Goeckede, M., Gogo, S., Gondwe, M. J., Goodrich, J. P.,
- Gottschalk, P., Graham, S. L., Heimann, M., Helbig, M., Helfter, C., Hemes, K. S., Hirano, T., Hollinger, D., Hörtnagl, L., Iwata, H., Jacotot, A., Jurasinski, G., Kang, M., Kasak, K., King, J., Klatt, J., Koebsch, F., Krauss, K. W., Lai, D. Y. F., Lohila, A., Mammarella, I., Belelli Marchesini, L., Manca, G., Matthes, J. H., Maximov, T., Merbold, L., Mitra, B., Morin, T. H., Nemitz, E., Nilsson, M. B., Niu, S., Oechel, W. C., Oikawa, P. Y., Ono, K., Peichl, M., Peltola, O., Reba, M. L., Richardson, A. D., Riley, W., Runkle, B. R. K., Ryu, Y., Sachs, T., Sakabe, A., Sanchez, C. R., Schuur, E. A., Schäfer, K. V. R., Sonnentag, O., Sparks, J. P., Stuart-Haëntjens, E., Sturtevant,
- C., Sullivan, R. C., Szutu, D. J., Thom, J. E., Torn, M. S., Tuittila, E.-S., Turner, J., Ueyama, M., Valach, A. C., Vargas, R., Varlagin, A., Vazquez-Lule, A., Verfaillie, J. G., Vesala, T., Vourlitis, G. L., Ward, E. J., Wille, C., Wohlfahrt, G., Wong, G. X., Zhang, Z., Zona, D., Windham-Myers, L., Poulter, B., and Jackson, R. B.: FLUXNET-CH4: A Global, Multi-Ecosystem Dataset and Analysis of Methane Seasonality from Freshwater Wetlands, Earth Syst. Sci. Data, 13, 3607–3689, https://doi.org/10.5194/essd-13-3607-2021, 2021.
- Drinkwater, A., Palmer, P. I., Feng, L., Arnold, T., Lan, X., Michel, S. E., Parker, R., and Boesch, H.: Atmospheric Data Support a Multi-Decadal Shift in the Global Methane Budget towards Natural Tropical Emissions, Atmospheric Chemistry and Physics, 23, 8429–8452, https://doi.org/10.5194/acp-23-8429-2023, 2023.
 - Ehret, G., Bousquet, P., Pierangelo, C., Alpers, M., Millet, B., Abshire, J. B., Bovensmann, H., Burrows, J. P., Chevallier, F., Ciais, P., Crevoisier, C., Fix, A., Flamant, P., Frankenberg, C., Gibert, F., Heim, B., Heimann, M., Houweling, S., Hubberten, H. W., Jöckel, P., Law, K., Löw, A., Marshall, J., Agusti-Panareda, A., Payan, S., Prigent, C., Rairoux, P., Sachs, T., Scholze, M., and Wirth, M.: MERLIN: A
- French-German Space Lidar Mission Dedicated to Atmospheric Methane, Remote Sensing, 9, 1052, https://doi.org/10.3390/rs9101052, 2017.
 - Etiope, G., Ciotoli, G., Schwietzke, S., and Schoell, M.: Gridded Maps of Geological Methane Emissions and Their Isotopic Signature, Earth System Science Data, 11, 1–22, https://doi.org/10.5194/essd-11-1-2019, 2019.
- Famiglietti, C. A., Smallman, T. L., Levine, P. A., Flack-Prain, S., Quetin, G. R., Meyer, V., Parazoo, N. C., Stettz, S. G., Yang, Y., Bonal, D.,

 Bloom, A. A., Williams, M., and Konings, A. G.: Optimal Model Complexity for Terrestrial Carbon Cycle Prediction, Biogeosciences,

 18, 2727–2754, https://doi.org/10.5194/bg-18-2727-2021, 2021.
 - Forster, G. and Manning, A.: Atmospheric CH4 Product, Weybourne (10.0 m), 2013-03-06–2024-03-31, https://doi.org/https://hdl.handle.net/11676/z7mpwPjyMPWI5aRv7eW52kMS, 2024.

- Forster, P. M., Smith, C. J., Walsh, T., Lamb, W. F., Lamboll, R., Hauser, M., Ribes, A., Rosen, D., Gillett, N., Palmer, M. D., Rogelj, J., von
 Schuckmann, K., Seneviratne, S. I., Trewin, B., Zhang, X., Allen, M., Andrew, R., Birt, A., Borger, A., Boyer, T., Broersma, J. A., Cheng, L., Dentener, F., Friedlingstein, P., Gutiérrez, J. M., Gütschow, J., Hall, B., Ishii, M., Jenkins, S., Lan, X., Lee, J.-Y., Morice, C., Kadow, C., Kennedy, J., Killick, R., Minx, J. C., Naik, V., Peters, G. P., Pirani, A., Pongratz, J., Schleussner, C.-F., Szopa, S., Thorne, P., Rohde, R., Rojas Corradi, M., Schumacher, D., Vose, R., Zickfeld, K., Masson-Delmotte, V., and Zhai, P.: Indicators of Global Climate Change 2022: Annual Update of Large-Scale Indicators of the State of the Climate System and Human Influence, Earth System Science Data, 15, 2295–2327, https://doi.org/10.5194/essd-15-2295-2023, 2023.
 - Gómez-Ortiz, C., Monteil, G., Basu, S., and Scholze, M.: Can $\Delta^{14}CO_2$ Observations Help Atmospheric Inversions Constrain the Fossil CO\$_2\$ Emission Budget of Europe?, EGUsphere, pp. 1–36, https://doi.org/10.5194/egusphere-2023-2215, 2023.
 - Gurney, K. R., Law, R. M., Denning, A. S., Rayner, P. J., Pak, B. C., Baker, D., Bousquet, P., Bruhwiler, L., Chen, Y.-H., Ciais, P., Fung, I. Y., Heimann, M., John, J., Maki, T., Maksyutov, S., Peylin, P., Prather, M., and Taguchi, S.: Transcom 3 Inversion Intercomparison:
- Model Mean Results for the Estimation of Seasonal Carbon Sources and Sinks, Global Biogeochemical Cycles, 18, 2003GB002111, https://doi.org/10.1029/2003GB002111, 2004.
 - Hammer, S. and Levin, I.: Atmospheric CH4 Product, Heidelberg (30.0 m), 1996-01-01-2024-03-31, https://doi.org/https://hdl.handle.net/11676/IIBrV9jz9D4hlHWVSbg1mMG_, 2024.
- Harris, I., Osborn, T. J., Jones, P., and Lister, D.: Version 4 of the CRU TS Monthly High-Resolution Gridded Multivariate Climate Dataset,

 Scientific Data, 7, 109, https://doi.org/10.1038/s41597-020-0453-3, 2020.
 - Hastings, W. K.: Monte Carlo Sampling Methods Using Markov Chains and Their Applications, Biometrika, 57, 97–109, https://doi.org/10.1093/biomet/57.1.97, 1970.
 - Haszpra, L.: Atmospheric CH4 at Hegyhátsál háttérszennyettség-mérő állomás by Institute for Nuclear Research, dataset published as CH4_HUN6034_tower-insitu_ATOMKI_tower82 at WDCGG, ver. 2025-01-01-0237, 2025.
- 790 Hatakka, J. and Laurila, T.: Atmospheric CH4 Product, Utö Baltic Sea (57.0 m), 2012-03-23-2024-03-31, https://doi.org/https://hdl.handle.net/11676/DIsAmw1ZIAmRJHNB_8dFN_jq, 2024.
 - Heliasz, M. and Biermann, T.: Atmospheric CH4 Product, Hyltemossa (150.0 m), 2016-12-13–2024-03-31, https://doi.org/https://hdl.handle.net/11676/dwFbNZQ1Y5_B6cZSkUopJbtm, 2024.
- Houweling, S., Bergamaschi, P., Chevallier, F., Heimann, M., Kaminski, T., Krol, M., Michalak, A. M., and Patra, P.: Global Inverse Modeling of CH₄ Sources and Sinks: An Overview of Methods, Atmospheric Chemistry and Physics, 17, 235–256, https://doi.org/10.5194/acp-17-235-2017, 2017.
 - ICOS RI, Aalto, J., Aalto, P., Aaltonen, H., Aiguier, T., Akubia, J., Ala-Könni, J., Alivernini, A., Aluome, C., Andersson, T., Arca, A., Arriga, N., Aurela, M., BRECHET, L., Baab, F., Back, J., Baltes, U., Baneschi, I., Barten, S., Baur, T., Bauters, M., Bazot, S., Beauclair, P., Becker, N., Belelli Marchesini, L., Bergström, G., Bernhofer, C., Berveiller, D., Biermann, T., Bignotti, L., Biron, R., Bloor, J., Bodson,
- B., Boeckx, P., Bogaerts, G., Bonal, D., Boon, G., Bornet, F., Bortoli, M., Bosio, I., Brut, A., Brümmer, C., Buchmann, N., Bulonza, E., Burban, B., Buysse, P., Båth, A., Calandrelli, D., Calvet, J.-C., Canut-Rocafort, G., Carrara, A., Cavagna, M., Ceschia, E., Chabbi, A., Chan, T., Chebbi, W., Chianucci, F., Chipeaux, C., Chopin, H., Christen, A., Chrysoulakis, N., Claverie, N., Cobbe, I., Cohard, J.-M., Colosse, D., Conte, A., Corsanici, R., Coulaud, C., Courtois, P., Coyle, M., Cremonese, E., Crill, P., Cuntz, M., Cuocolo, D., Czerný, R., DEPUYDT, J., Daelman, R., Darenová, E., Darsonville, O., De Ligne, A., De Meulder, T., De Simon, G., Decau, M.-L., Dell'Acqua,
- A., Delorme, J.-P., Delpierre, N., Demoulin, L., Denou, J.-L., Di Tommasi, P., Dienstbach, L., Dignam, R., Dolfus, D., Domec, J.-C., Douxfils, B., Drösler, M., Drüe, C., Dufrêne, E., Dumont, B., Durand, B., Dusek, J., Eberl, J., Eichelmann, U., Ekili, D., Engelmann, T.,

- Esposito, A., Esser, O., Etienne, J.-C., Etzold, S., Eugster, W., Famulari, D., Fares, S., Faurès, A., Fauvel, Y., Feigenwinter, I., Feldmann, I., Fincham, W., Finco, A., Fischer, M., Flechard, C., Foltýnová, L., Foulquier, A., Friborg, T., Galliot, J.-N., Galvagno, M., Garcia Quiros, I., Garrigou, C., Gastal, F., Geilfus, N.-X., Gerosa, G., Gessler, A., Gharun, M., Giamberini, M., Gianelle, D., Gibrin, H., Gimper, S., 810 Goded, I., Graf, A., Granouillac, F., Grehan, E., Grenier, M., Grudd, H., Grünwald, T., Guillot, T., Hamon, Y., Harvey, D., Hatakka, J., Haustein, A., Hehn, M., Heinesch, B., Helfter, C., Heliasz, M., Holst, J., Holst, T., Holtmann, A., Hug, C., Huguet, C., Häni, M., Hörtnagl, L., Ibrom, A., Ilardi, F., Jackowicz-Korczynski, M. A., Jacotot, A., Janssens, I., Jensen, R., Jocher, G., Joetzjer, E., Jones, M., Järvi, L., Kempf, J., Keronen, P., Kettler, M., Kimbesa, F., Kivalov, S., Klatt, J., Kljun, N., Klosterhalfen, A., Klumpp, K., Knohl, A., Kogxylakis, G., Kolari, P., Kolbe, S., Korkiakoski, M., Korrensalo, A., Kowalska, N., Kozii, N., Kreiza, J., Kristoffersson, A., Kruiit, B., Kruszewski, A., Kulmala, L., Kumar, S., Kummer, S., Laakso, H., Lafont, S., Lange Rønn, E., Larmanou, E., Laurila, T., Leeson, S., Lefevre, L., 815 Lehner, I., Lemaire, B., Leonard, J., Levula, J., Levy, P., Liechti, K., Liger, L., Lily, J.-B., Limousin, J.-M., Linderson, M.-L., Lindgren, K., Lo Cascio, M., Lohila, A., Longdoz, B., Lootens, R., Loubet, B., Loustau, D., Lucarini, A., Lundin, E., López-Blanco, E., Löfvenius, P., Magliulo, V., Mammarella, I., Manco, A., Manise, T., Marcolla, B., Marek, M. V., Marklund, P., Markwitz, C., Marloie, O., Marras, S., Martin, R., Martin - Saint Paul, N., Marty, M., Martín, M. P., Marzuoli, R., Matilainen, T., Mattes, J., Matteucci, M., Mauder, M., 820 Maurel, W., Mbifo, J., Meggio, F., Meier, F., Meier, P., Meire, A., Meis, J., Mensah, C., Meyer, H., Michaud, L., Minerbi, S., Moderow, U., Montagnani, L., Moreno, G., Moretti, V., Morfin, A., Morra di Cella, U., Mullinger, N., Mäkelä, T., Männikkö, M., Männistö, E., Mölder, M., Møller, F., Naiken, A., Naseer, M., Nemitz, E., Nezval, O., Nilsson, M., Norkko, J., Ocallaghan, F., Ojala, A., Orgun, A., Ottosson-Löfvenius, M., Ourcival, J.-M., Paasch, S., Paci, A., Pavelka, M., Pavot, L., Peichl, M., Peressotti, A., Perot-Guillaume, C., Perrot, C., Pihlatie, M., Pilegaard, K., Pilkottu, R., Piret, A., Pitacco, A., Plapp, T., Plebani, D., Politakos, K., Prasse, H., Provenzale, 825 A., Pumpanen, J., Raco, B., Rainne, J., Rakos, N., Rasmussen, L., Rebmann, C., Redepenning, D., Rinne, J., Rodeghiero, M., Roland, M., Rudd, D., Røjle Christensen, T., Sahoo, G., Salze, P., Schaarup Sørensen, J., Schindler, D., Schlaipfer, M., Schmidt, P., Schmitt Oehler, M., Schrader, F., Segers, J., Sibret, T., Siebicke, L., Siivola, E., Simioni, G., Sirca, C., Smith, P., Snellen, H., Sorgi, T., Soudani, K., Spano, D., Spence, K., Spyridakis, N., Stagakis, S., Staník, K., Staudinger, M., Stecher, M., Stellner, S., Stutz, T., Suopajärvi, S., Sutter, F., Taipale, R., Tallec, T., Tenca, F., Tezza, L., Thimonier Rickenmann, A., Thyrion, T., Tiedemann, F., Tomelleri, E., Trotsiuk, 830 V., Trusina, J., Tuittila, E.-S., Tuovinen, J.-P., Tyssandier, J., Valay, J.-G., Van Damme, F., Van Look, J., Varjonen, S., Vendrame, N., Verbeeck, H., Vesala, T., Vescovo, L., Vincent, G., Vincke, C., Vitale, L., Vivaldo, G., Voisin, D., Vágner, L., Vähä, A., Waldner, P., Wiesen, R., Winck, B., Yeung, K., Zampedri, R., Zawilski, B., Zenone, T., Zimmermann, S., Zweifel, R., de Berranger, C., van Dijk, N.,
- Ioannidis, E., Meesters, A., Steiner, M., Brunner, D., Reum, F., Pison, I., Berchet, A., Thompson, R., Sollum, E., Koch, F.-T., Gerbig, C., Wang, F., Maksyutov, S., Tsuruta, A., Tenkanen, M., Aalto, T., Monteil, G., Lin, H., Ren, G., Scholze, M., and Houweling, S.:

 An inter-comparison of inverse models for estimating European CH₄ emissions, Earth System Science Data Discussions, pp. 1–42, https://doi.org/10.5194/essd-2025-235, publisher: Copernicus GmbH, 2025.

https://doi.org/10.18160/G5KZ-ZD83, 2024.

van der Molen, M., Šigut, L., Šlížek, J., and ICOS ETC: Ecosystem Final Quality (L2) Product in ETC-Archive Format - Release 2024-1,

- Ishizawa, M., Chan, D., Worthy, D., Chan, E., Vogel, F., Melton, J. R., and Arora, V. K.: Estimation of Canada's Methane Emissions: Inverse

 Modelling Analysis Using the ECCC Measurement Network, https://doi.org/10.5194/egusphere-2023-2550, 2023.
 - Ito, A., Li, T., Qin, Z., Melton, J. R., Tian, H., Kleinen, T., Zhang, W., Zhang, Z., Joos, F., Ciais, P., Hopcroft, P. O., Beerling, D. J., Liu, X., Zhuang, Q., Zhu, Q., Peng, C., Chang, K.-Y., Fluet-Chouinard, E., McNicol, G., Patra, P., Poulter, B., Sitch, S., Riley, W., and Zhu, Q.: Cold-Season Methane Fluxes Simulated by GCP-CH4 Models, Geophysical Research Letters, 50, e2023GL103037, https://doi.org/10.1029/2023GL103037, 2023.

Johnson, M. S., Matthews, E., Du, J., Genovese, V., and Bastviken, D.: Methane Emission From Global Lakes: New Spatiotemporal Data and Observation-Driven Modeling of Methane Dynamics Indicates Lower Emissions, Journal of Geophysical Research: Biogeosciences, 127, e2022JG006793, https://doi.org/10.1029/2022JG006793, 2022.

- Kallingal, J. T., Lindström, J., Miller, P. A., Rinne, J., Raivonen, M., and Scholze, M.: Optimising CH₄ simulations from the LPJ-GUESS model v4.1 using an adaptive Markov chain Monte Carlo algorithm, Geoscientific Model Development, 17, 2299–2324, https://doi.org/10.5194/gmd-17-2299-2024, publisher: Copernicus GmbH, 2024a.
- Kallingal, J. T., Scholze, M., Miller, P. A., Lindström, J., Rinne, J., Aurela, M., Vestin, P., and Weslien, P.: Assimilating Multi-site Eddy-Covariance Data to Calibrate the CH₄ Wetland Emission Module in a Terrestrial Ecosystem Model, EGUsphere, pp. 1–32, https://doi.org/10.5194/egusphere-2024-373, 2024b.
- Kirschke, S., Bousquet, P., Ciais, P., Saunois, M., Canadell, J. G., Dlugokencky, E. J., Bergamaschi, P., Bergmann, D., Blake, D. R., Bruhwiler,
 L., Cameron-Smith, P., Castaldi, S., Chevallier, F., Feng, L., Fraser, A., Heimann, M., Hodson, E. L., Houweling, S., Josse, B., Fraser, P. J.,
 Krummel, P. B., Lamarque, J.-F., Langenfelds, R. L., Le Quéré, C., Naik, V., O'Doherty, S., Palmer, P. I., Pison, I., Plummer, D., Poulter,
 B., Prinn, R. G., Rigby, M., Ringeval, B., Santini, M., Schmidt, M., Shindell, D. T., Simpson, I. J., Spahni, R., Steele, L. P., Strode, S. A.,
 Sudo, K., Szopa, S., van der Werf, G. R., Voulgarakis, A., van Weele, M., Weiss, R. F., Williams, J. E., and Zeng, G.: Three Decades of
 Global Methane Sources and Sinks, Nature Geoscience, 6, 813–823, https://doi.org/10.1038/ngeo1955, 2013.
- Knorr, W. and Heimann, M.: Impact of Drought Stress and Other Factors on Seasonal Land Biosphere CO2 Exchange Studied through an Atmospheric Tracer Transport Model, Tellus B, 47, 471–489, https://doi.org/10.1034/j.1600-0889.47.issue4.7.x, 1995.
 - Kubistin, D., Plaß-Dülmer, C., Arnold, S., Kneuer, T., Lindauer, M., Müller-Williams, J., and Schumacher, M.: Atmospheric CH4 Product, Torfhaus (147.0 m), 2017-12-12-2024-03-31, https://doi.org/https://hdl.handle.net/11676/3oT_XC6YHxBDG3NmNZ-SMisB, 2024a.
- Kubistin, D., Plaß-Dülmer, C., Arnold, S., Kneuer, T., Lindauer, M., Müller-Williams, J., and Schumacher, M.: Atmospheric CH4 Product, Hohenpeissenberg (131.0 m), 2015-09-03–2024-03-31, https://doi.org/https://hdl.handle.net/11676/WTBfJCTsxRUtjo2jsvO2277I, 2024b.
 - Kubistin, D., Plaß-Dülmer, C., Arnold, S., Kneuer, T., Lindauer, M., Müller-Williams, J., and Schumacher, M.: Atmospheric CH4 Product, Lindenberg (98.0 m), 2015-10-08–2024-03-31, https://doi.org/https://hdl.handle.net/11676/fH0UqKnX7rf_kigEjawJ9Adk, 2024c.
- Laitinen, A., Aaltonen, H., Zellweger, C., Tsuruta, A., Aalto, T., and Hatakka, J.: Long-term observations of atmospheric CO₂ and CH₄ trends and comparison of two measurement systems at Pallas-Sammaltunturi station in Northern Finland, Atmospheric Measurement Techniques, 18, 3109–3133, https://doi.org/10.5194/amt-18-3109-2025, publisher: Copernicus GmbH, 2025.
 - Lan, X., Mund, J., Crotwell, A., Thoning, K., Moglia, E., Madronich, M., Baugh, K., Petron, G., Crotwell, M., Neff, D., Wolter, S., Mefford, T., and Devogel, S.: Atmospheric Methane Dry Air Mole Fractions from the NOAA GML Carbon Cycle Cooperative Global Air Sampling Network, 1983-2023, https://doi.org/10.15138/VNCZ-M766, 2025.
- Lanczos, C.: Solution of Systems of Linear Equations by Minimized Iterations, Journal of Research of the National Bureau of Standards, 49, 33, https://doi.org/10.6028/jres.049.006, 1952.
 - Lehner, I. and Mölder, M.: Atmospheric CH4 Product, Norunda (100.0 m), 2017-01-31–2024-03-31, https://doi.org/https://hdl.handle.net/11676/dyPHK7qEEbQFnqSJx8ZntxOI, 2024.
- Levula, J. and Mammarella, I.: Atmospheric CH4 Product, Hyytiälä (125.0 m), 2015-05-03–2024-03-31, https://doi.org/https://hdl.handle.net/11676/oMPibudu556XoynXRXnqLilC, 2024.
 - Lopez, M. and Ramonet, M.: Atmospheric CH4 Product, Biscarrosse (47.0 m), 2009-09-01-2024-03-31, https://doi.org/https://hdl.handle.net/11676/Hdn5JfclbuA3xIdcF2oW_Jf0, 2024.

- Lunder, C. and Platt, S.: Main Greenhouse Gases and Carbon_monoxide at Birkenes II, https://doi.org/10.48597/77S6-364A, 2025.
- Mahadevan, P., Wofsy, S. C., Matross, D. M., Xiao, X., Dunn, A. L., Lin, J. C., Gerbig, C., Munger, J. W., Chow, V. Y., and Gottlieb, E. W.: A Satellite-Based Biosphere Parameterization for Net Ecosystem CO2 Exchange: Vegetation Photosynthesis and Respiration Model (VPRM), Global Biogeochemical Cycles, 22, https://doi.org/10.1029/2006GB002735, 2008.
 - Marek, M. V., Vítková, G., and Komínková, K.: Atmospheric CH4 Product, Křešín u Pacova (250.0 m), 2017-04-12–2024-03-31, https://doi.org/https://hdl.handle.net/11676/ft2De4_2elQIT8nyj0_6TYsW, 2024.
- McGuire, A. D., Christensen, T. R., Hayes, D., Heroult, A., Euskirchen, E., Kimball, J. S., Koven, C., Lafleur, P., Miller, P. A., Oechel, W.,
 Peylin, P., Williams, M., and Yi, Y.: An Assessment of the Carbon Balance of Arctic Tundra: Comparisons among Observations, Process
 Models, and Atmospheric Inversions, Biogeosciences, 9, 3185–3204, https://doi.org/10.5194/bg-9-3185-2012, 2012.
 - McNicol, G., Fluet-Chouinard, E., Ouyang, Z., Knox, S., Zhang, Z., Aalto, T., Bansal, S., Chang, K.-Y., Chen, M., Delwiche, K., Feron, S., Goeckede, M., Liu, J., Malhotra, A., Melton, J. R., Riley, W., Vargas, R., Yuan, K., Ying, Q., Zhu, Q., Alekseychik, P., Aurela, M., Billesbach, D. P., Campbell, D. I., Chen, J., Chu, H., Desai, A. R., Euskirchen, E., Goodrich, J., Griffis, T., Hel-
- big, M., Hirano, T., Iwata, H., Jurasinski, G., King, J., Koebsch, F., Kolka, R., Krauss, K., Lohila, A., Mammarella, I., Nilson, M., Noormets, A., Oechel, W., Peichl, M., Sachs, T., Sakabe, A., Schulze, C., Sonnentag, O., Sullivan, R. C., Tuittila, E.-S., Ueyama, M., Vesala, T., Ward, E., Wille, C., Wong, G. X., Zona, D., Windham-Myers, L., Poulter, B., and Jackson, R. B.: Upscaling Wetland Methane Emissions From the FLUXNET-CH4 Eddy Covariance Network (UpCH4 v1.0): Model Development, Network Assessment, and Budget Comparison, AGU Advances, 4, e2023AV000956, https://doi.org/10.1029/2023AV000956, _eprint: https://agupubs.onlinelibrary.wiley.com/doi/pdf/10.1029/2023AV000956, 2023.
 - Meinhardt, F.: Atmospheric CH4 at Schauinsland by German Environment Agency, dataset published as CH4_SSL6027_surface-insitu_UBAG_data1 at WDCGG, ver. 2025-01-01-0111, 2025.
 - Melton, J. R., Wania, R., Hodson, E. L., Poulter, B., Ringeval, B., Spahni, R., Bohn, T., Avis, C. A., Beerling, D. J., Chen, G., Eliseev, A. V., Denisov, S. N., Hopcroft, P. O., Lettenmaier, D. P., Riley, W. J., Singarayer, J. S., Subin, Z. M., Tian, H., Zürcher, S., Brovkin, V., van Bodegom, P. M., Kleinen, T., Yu, Z. C., and Kaplan, J. O.: Present State of Global Wetland Extent and Wetland Methane Modelling: Conclusions from a Model Inter-Comparison Project (WETCHIMP), Biogeosciences, 10, 753–788, https://doi.org/10.5194/bg-10-753-2013, 2013.

905

- Metropolis, N., Rosenbluth, A. W., Rosenbluth, M. N., Teller, A. H., and Teller, E.: Equation of State Calculations by Fast Computing Machines, The Journal of Chemical Physics, 21, 1087–1092, https://doi.org/10.1063/1.1699114, 1953.
- 910 Monteil, G. and Scholze, M.: Regional CO₂ Inversions with LUMIA, the Lund University Modular Inversion Algorithm, v1.0, Geoscientific Model Development, 14, 3383–3406, https://doi.org/10.5194/gmd-14-3383-2021, 2021.
 - Monteil, G., Broquet, G., Scholze, M., Lang, M., Karstens, U., Gerbig, C., Koch, F.-T., Smith, N. E., Thompson, R. L., Luijkx, I. T., White, E., Meesters, A., Ciais, P., Ganesan, A. L., Manning, A., Mischurow, M., Peters, W., Peylin, P., Tarniewicz, J., Rigby, M., Rödenbeck, C., Vermeulen, A., and Walton, E. M.: The Regional European Atmospheric Transport Inversion Comparison, EUROCOM: First Results on European-wide Terrestrial Carbon Fluxes for the Period 2006–2015, Atmospheric Chemistry and Physics, 20, 12063–12091, https://doi.org/10.5194/acp-20-12063-2020, 2020.
 - Müller, J. and Joos, F.: Global Peatland Area and Carbon Dynamics from the Last Glacial Maximum to the Present a Process-Based Model Investigation, Biogeosciences, 17, 5285–5308, https://doi.org/10.5194/bg-17-5285-2020, 2020.

- Munassar, S., Monteil, G., Scholze, M., Karstens, U., Rödenbeck, C., Koch, F.-T., Totsche, K. U., and Gerbig, C.: Why Do Inverse Models Disagree? A Case Study with Two European CO₂ Inversions, Atmospheric Chemistry and Physics, 23, 2813–2828, https://doi.org/10.5194/acp-23-2813-2023, 2023.
 - Nesser, H., Jacob, D. J., Maasakkers, J. D., Lorente, A., Chen, Z., Lu, X., Shen, L., Qu, Z., Sulprizio, M. P., Winter, M., Ma, S., Bloom, A. A., Worden, J. R., Stavins, R. N., and Randles, C. A.: High-Resolution US Methane Emissions Inferred from an Inversion of 2019 TROPOMI Satellite Data: Contributions from Individual States, Urban Areas, and Landfills, Atmospheric Chemistry and Physics, 24, 5069–5091, https://doi.org/10.5194/acp-24-5069-2024, 2024.

- Nisbet, E. G., Dlugokencky, E. J., Manning, M. R., Lowry, D., Fisher, R. E., France, J. L., Michel, S. E., Miller, J. B., White, J. W. C., Vaughn, B., Bousquet, P., Pyle, J. A., Warwick, N. J., Cain, M., Brownlow, R., Zazzeri, G., Lanoisellé, M., Manning, A. C., Gloor, E., Worthy, D. E. J., Brunke, E.-G., Labuschagne, C., Wolff, E. W., and Ganesan, A. L.: Rising Atmospheric Methane: 2007–2014 Growth and Isotopic Shift, Global Biogeochemical Cycles, 30, 1356–1370, https://doi.org/10.1002/2016GB005406, 2016.
- 930 O'Doherty, S. and Pitt, J.: Atmospheric CH4 Product, Tacolneston (185.0 m), 2013-01-31–2024-03-31, https://doi.org/https://hdl.handle.net/11676/sGoYLTdK6BmrBm1mBKgA0uoD, 2024.
 - O'Doherty, S., Pitt, J., and Stanley, K.: Atmospheric CH4 Product, Ridge Hill (90.0 m), 2012-02-23-2024-03-31, https://doi.org/https://hdl.handle.net/11676/XENJWmI0eRV4pNf2xrLFt5SR, 2024.
- Pastorello, G., Trotta, C., Canfora, E., Chu, H., Christianson, D., Cheah, Y.-W., Poindexter, C., Chen, J., Elbashandy, A., Humphrey, M.,
 Isaac, P., Polidori, D., Reichstein, M., Ribeca, A., van Ingen, C., Vuichard, N., Zhang, L., Amiro, B., Ammann, C., Arain, M. A., Ardö, J.,
 Arkebauer, T., Arndt, S. K., Arriga, N., Aubinet, M., Aurela, M., Baldocchi, D., Barr, A., Beamesderfer, E., Marchesini, L. B., Bergeron,
 O., Beringer, J., Bernhofer, C., Berveiller, D., Billesbach, D., Black, T. A., Blanken, P. D., Bohrer, G., Boike, J., Bolstad, P. V., Bonal, D.,
 Bonnefond, J.-M., Bowling, D. R., Bracho, R., Brodeur, J., Brümmer, C., Buchmann, N., Burban, B., Burns, S. P., Buysse, P., Cale, P.,
 Cavagna, M., Cellier, P., Chen, S., Chini, I., Christensen, T. R., Cleverly, J., Collalti, A., Consalvo, C., Cook, B. D., Cook, D., Coursolle, C.,
- Cremonese, E., Curtis, P. S., D'Andrea, E., da Rocha, H., Dai, X., Davis, K. J., Cinti, B. D., de Grandcourt, A., Ligne, A. D., De Oliveira, R. C., Delpierre, N., Desai, A. R., Di Bella, C. M., di Tommasi, P., Dolman, H., Domingo, F., Dong, G., Dore, S., Duce, P., Dufrêne, E., Dunn, A., Dušek, J., Eamus, D., Eichelmann, U., ElKhidir, H. A. M., Eugster, W., Ewenz, C. M., Ewers, B., Famulari, D., Fares, S., Feigenwinter, I., Feitz, A., Fensholt, R., Filippa, G., Fischer, M., Frank, J., Galvagno, M., Gharun, M., Gianelle, D., Gielen, B., Gioli, B., Gitelson, A., Goded, I., Goeckede, M., Goldstein, A. H., Gough, C. M., Goulden, M. L., Graf, A., Griebel, A., Gruening, C., Grünwald,
- T., Hammerle, A., Han, S., Han, X., Hansen, B. U., Hanson, C., Hatakka, J., He, Y., Hehn, M., Heinesch, B., Hinko-Najera, N., Hörtnagl, L., Hutley, L., Ibrom, A., Ikawa, H., Jackowicz-Korczynski, M., Janouš, D., Jans, W., Jassal, R., Jiang, S., Kato, T., Khomik, M., Klatt, J., Knohl, A., Knox, S., Kobayashi, H., Koerber, G., Kolle, O., Kosugi, Y., Kotani, A., Kowalski, A., Kruijt, B., Kurbatova, J., Kutsch, W. L., Kwon, H., Launiainen, S., Laurila, T., Law, B., Leuning, R., Li, Y., Liddell, M., Limousin, J.-M., Lion, M., Liska, A. J., Lohila, A., López-Ballesteros, A., López-Blanco, E., Loubet, B., Loustau, D., Lucas-Moffat, A., Lüers, J., Ma, S., Macfarlane, C., Magliulo, V.,
- Maier, R., Mammarella, I., Manca, G., Marcolla, B., Margolis, H. A., Marras, S., Massman, W., Mastepanov, M., Matamala, R., Matthes, J. H., Mazzenga, F., McCaughey, H., McHugh, I., McMillan, A. M. S., Merbold, L., Meyer, W., Meyers, T., Miller, S. D., Minerbi, S., Moderow, U., Monson, R. K., Montagnani, L., Moore, C. E., Moors, E., Moreaux, V., Moureaux, C., Munger, J. W., Nakai, T., Neirynck, J., Nesic, Z., Nicolini, G., Noormets, A., Northwood, M., Nosetto, M., Nouvellon, Y., Novick, K., Oechel, W., Olesen, J. E., Ourcival, J.-M., Papuga, S. A., Parmentier, F.-J., Paul-Limoges, E., Pavelka, M., Peichl, M., Pendall, E., Phillips, R. P., Pilegaard, K., Pirk, N., Posse, G.,
- Powell, T., Prasse, H., Prober, S. M., Rambal, S., Rannik, Ü., Raz-Yaseef, N., Rebmann, C., Reed, D., de Dios, V. R., Restrepo-Coupe, N., Reverter, B. R., Roland, M., Sabbatini, S., Sachs, T., Saleska, S. R., Sánchez-Cañete, E. P., Sanchez-Mejia, Z. M., Schmid, H. P., Schmidt,

- M., Schneider, K., Schrader, F., Schroder, I., Scott, R. L., Sedlák, P., Serrano-Ortíz, P., Shao, C., Shi, P., Shironya, I., Siebicke, L., Šigut, L., Silberstein, R., Sirca, C., Spano, D., Steinbrecher, R., Stevens, R. M., Sturtevant, C., Suyker, A., Tagesson, T., Takanashi, S., Tang, Y., Tapper, N., Thom, J., Tomassucci, M., Tuovinen, J.-P., Urbanski, S., Valentini, R., van der Molen, M., van Gorsel, E., van Huissteden,
- K., Varlagin, A., Verfaillie, J., Vesala, T., Vincke, C., Vitale, D., Vygodskaya, N., Walker, J. P., Walter-Shea, E., Wang, H., Weber, R., Westermann, S., Wille, C., Wofsy, S., Wohlfahrt, G., Wolf, S., Woodgate, W., Li, Y., Zampedri, R., Zhang, J., Zhou, G., Zona, D., Agarwal, D., Biraud, S., Torn, M., and Papale, D.: The FLUXNET2015 Dataset and the ONEFlux Processing Pipeline for Eddy Covariance Data, Scientific Data, 7, 225, https://doi.org/10.1038/s41597-020-0534-3, 2020.
- Peltola, O., Vesala, T., Gao, Y., Räty, O., Alekseychik, P., Aurela, M., Chojnicki, B., Desai, A. R., Dolman, A. J., Euskirchen, E. S., Friborg, T.,
 Göckede, M., Helbig, M., Humphreys, E., Jackson, R. B., Jocher, G., Joos, F., Klatt, J., Knox, S. H., Kowalska, N., Kutzbach, L., Lienert, S., Lohila, A., Mammarella, I., Nadeau, D. F., Nilsson, M. B., Oechel, W. C., Peichl, M., Pypker, T., Quinton, W., Rinne, J., Sachs, T., Samson, M., Schmid, H. P., Sonnentag, O., Wille, C., Zona, D., and Aalto, T.: Monthly Gridded Data Product of Northern Wetland Methane Emissions Based on Upscaling Eddy Covariance Observations, Earth System Science Data, 11, 1263–1289, https://doi.org/10.5194/essd-11-1263-2019, 2019.
- Peng, S., Lin, X., Thompson, R. L., Xi, Y., Liu, G., Hauglustaine, D., Lan, X., Poulter, B., Ramonet, M., Saunois, M., Yin, Y., Zhang, Z., Zheng, B., and Ciais, P.: Wetland Emission and Atmospheric Sink Changes Explain Methane Growth in 2020, Nature, 612, 477–482, https://doi.org/10.1038/s41586-022-05447-w, 2022.
 - Pisso, I., Sollum, E., Grythe, H., Kristiansen, N. I., Cassiani, M., Eckhardt, S., Arnold, D., Morton, D., Thompson, R. L., Groot Zwaaftink, C. D., Evangeliou, N., Sodemann, H., Haimberger, L., Henne, S., Brunner, D., Burkhart, J. F., Fouilloux, A., Brioude, J., Philipp, A.,
- 975 Seibert, P., and Stohl, A.: The Lagrangian Particle Dispersion Model FLEXPART Version 10.4, Geoscientific Model Development, 12, 4955–4997, https://doi.org/10.5194/gmd-12-4955-2019, 2019.
 - Potter, C. S., Randerson, J. T., Field, C. B., Matson, P. A., Vitousek, P. M., Mooney, H. A., and Klooster, S. A.: Terrestrial Ecosystem Production: A Process Model Based on Global Satellite and Surface Data, Global Biogeochemical Cycles, 7, 811–841, https://doi.org/10.1029/93GB02725, 1993.
- Prinn, R. G., Weiss, R. F., Arduini, J., Arnold, T., DeWitt, H. L., Fraser, P. J., Ganesan, A. L., Gasore, J., Harth, C. M., Hermansen, O., Kim, J., Krummel, P. B., Li, S., Loh, Z. M., Lunder, C. R., Maione, M., Manning, A. J., Miller, B. R., Mitrevski, B., Mühle, J., O'Doherty, S., Park, S., Reimann, S., Rigby, M., Saito, T., Salameh, P. K., Schmidt, R., Simmonds, P. G., Steele, L. P., Vollmer, M. K., Wang, R. H., Yao, B., Yokouchi, Y., Young, D., and Zhou, L.: History of Chemically and Radiatively Important Atmospheric Gases from the Advanced Global Atmospheric Gases Experiment (AGAGE), Earth System Science Data, 10, 985–1018, https://doi.org/10.5194/essd-10-985-2018,
 2018.
 - Qu, Z., Jacob, D. J., Zhang, Y., Shen, L., Varon, D. J., Lu, X., Scarpelli, T., Bloom, A., Worden, J., and Parker, R. J.: Attribution of the 2020 Surge in Atmospheric Methane by Inverse Analysis of GOSAT Observations, Environmental Research Letters, 17, 094 003, https://doi.org/10.1088/1748-9326/ac8754, 2022.
- Ramonet, M., Conil, S., Delmotte, M., Laurent, O., and Lopez, M.: Atmospheric CH4 Product, Observatoire Pérenne de l'environnement (120.0 m), 2011-04-21-2024-03-31, https://doi.org/https://hdl.handle.net/11676/25_LcWRQe-7rZpujELUKBeub, 2024a.
 - Ramonet, M., Delmotte, M., and Lopez, M.: Atmospheric CH4 Product, Saclay (100.0 m), 2015-07-08-2024-03-31, https://doi.org/https://hdl.handle.net/11676/dWDZTRzDW70ontXITF20DeUu, 2024b.
 - Ramonet, M., Lopez, M., and Delmotte, M.: Atmospheric CH4 Product, Trainou (180.0 m), 2007-01-29–2024-03-31, https://doi.org/https://hdl.handle.net/11676/5KUsuilZhUjFtzVEiusE60x_, 2024c.

- 995 Randerson, J., Van Der Werf, G., Giglio, L., Collatz, G., and Kasibhatla, P.: Global Fire Emissions Database, Version 4.1 (GFEDv4), https://doi.org/10.3334/ORNLDAAC/1293, 2017.
 - Rayner, P. J., Scholze, M., Knorr, W., Kaminski, T., Giering, R., and Widmann, H.: Two Decades of Terrestrial Carbon Fluxes from a Carbon Cycle Data Assimilation System (CCDAS), Global Biogeochemical Cycles, 19, https://doi.org/10.1029/2004GB002254, 2005.
- Rödenbeck, C., Gerbig, C., Trusilova, K., and Heimann, M.: A Two-Step Scheme for High-Resolution Regional Atmospheric Trace Gas

 Inversions Based on Independent Models, Atmospheric Chemistry and Physics, 9, 5331–5342, https://doi.org/10.5194/acp-9-5331-2009,
 2009.
 - Ross, S., Wang, H., Zheng, H., Yan, T., and Shirali, M.: Approaches for predicting dairy cattle methane emissions: from traditional methods to machine learning, Journal of Animal Science, 102, skae219, https://doi.org/10.1093/jas/skae219, 2024.
- Saunois, M., Stavert, A. R., Poulter, B., Bousquet, P., Canadell, J. G., Jackson, R. B., Raymond, P. A., Dlugokencky, E. J., Houweling, S.,
 Patra, P. K., Ciais, P., Arora, V. K., Bastviken, D., Bergamaschi, P., Blake, D. R., Brailsford, G., Bruhwiler, L., Carlson, K. M., Carrol, M., Castaldi, S., Chandra, N., Crevoisier, C., Crill, P. M., Covey, K., Curry, C. L., Etiope, G., Frankenberg, C., Gedney, N., Hegglin, M. I., Höglund-Isaksson, L., Hugelius, G., Ishizawa, M., Ito, A., Janssens-Maenhout, G., Jensen, K. M., Joos, F., Kleinen, T., Krummel, P. B., Langenfelds, R. L., Laruelle, G. G., Liu, L., Machida, T., Maksyutov, S., McDonald, K. C., McNorton, J., Miller, P. A., Melton, J. R., Morino, I., Müller, J., Murguia-Flores, F., Naik, V., Niwa, Y., Noce, S., O'Doherty, S., Parker, R. J., Peng, C., Peng, S., Peters, G. P.,
- Prigent, C., Prinn, R., Ramonet, M., Regnier, P., Riley, W. J., Rosentreter, J. A., Segers, A., Simpson, I. J., Shi, H., Smith, S. J., Steele, L. P., Thornton, B. F., Tian, H., Tohjima, Y., Tubiello, F. N., Tsuruta, A., Viovy, N., Voulgarakis, A., Weber, T. S., van Weele, M., van der Werf, G. R., Weiss, R. F., Worthy, D., Wunch, D., Yin, Y., Yoshida, Y., Zhang, W., Zhang, Z., Zhao, Y., Zheng, B., Zhu, Q., Zhu, Q., and Zhuang, Q.: The Global Methane Budget 2000–2017, Earth System Science Data, 12, 1561–1623, https://doi.org/10.5194/essd-12-1561-2020, 2020.
- 1015 Segers, A.: Description of the CH4 Inversion Production Chain, ECMWF Copernicus report, ECMWF, 2020.

- Sierk, B., Fernandez, V., Bézy, J.-L., Meijer, Y., Durand, Y., Courrèges-Lacoste, G. B., Pachot, C., Löscher, A., Nett, H., Minoglou, K., Boucher, L., Windpassinger, R., Pasquet, A., Serre, D., and te Hennepe, F.: The Copernicus CO2M Mission for Monitoring Anthropogenic Carbon Dioxide Emissions from Space, in: International Conference on Space Optics ICSO 2020, vol. 11852, pp. 1563–1580, SPIE, https://doi.org/10.1117/12.2599613, 2021.
- 1020 Sitch, S., Smith, B., Prentice, I. C., Arneth, A., Bondeau, A., Cramer, W., Kaplan, J. O., Levis, S., Lucht, W., Sykes, M. T., Thonicke, K., and Venevsky, S.: Evaluation of Ecosystem Dynamics, Plant Geography and Terrestrial Carbon Cycling in the LPJ Dynamic Global Vegetation Model, Global Change Biology, 9, 161–185, https://doi.org/10.1046/j.1365-2486.2003.00569.x, 2003.
 - Smith, B., Prentice, I. C., and Sykes, M. T.: Representation of Vegetation Dynamics in the Modelling of Terrestrial Ecosystems: Comparing Two Contrasting Approaches within European Climate Space, Global Ecology & Biogeography, pp. 621–237, 2001.
- Smith, B., Wårlind, D., Arneth, A., Hickler, T., Leadley, P., Siltberg, J., and Zaehle, S.: Implications of Incorporating N Cycling and N Limitations on Primary Production in an Individual-Based Dynamic Vegetation Model, Biogeosciences, 11, 2027–2054, https://doi.org/10.5194/bg-11-2027-2014, 2014.
 - Solazzo, E., Crippa, M., Guizzardi, D., Muntean, M., Choulga, M., and Janssens-Maenhout, G.: Uncertainties in the Emissions Database for Global Atmospheric Research (EDGAR) Emission Inventory of Greenhouse Gases, Atmospheric Chemistry and Physics, 21, 5655–5683, https://doi.org/10.5194/acp-21-5655-2021, 2021.

- Steinbacher, M.: Atmospheric CH4 at Jungfraujoch by Swiss Federal Laboratories for Materials Science and Technology, dataset published as CH4_JFJ6036_surface-insitu_Empa_data1 at WDCGG, ver. 2025-07-08-1503, https://doi.org/10.50849/WDCGG_0023-6036-1002-01-01-9999, 2018.
- Steiner, M., Peters, W., Luijkx, I., Henne, S., Chen, H., Hammer, S., and Brunner, D.: European CH₄ Inversions with ICON-ART Coupled to the CarbonTracker Data Assimilation Shell, Atmospheric Chemistry and Physics, 24, 2759–2782, https://doi.org/10.5194/acp-24-2759-2024, 2024.
 - Thanwerdas, J., Saunois, M., Berchet, A., Pison, I., and Bousquet, P.: Investigation of the Renewed Methane Growth Post-2007 with High-Resolution 3-D Variational Inverse Modeling and Isotopic Constraints, Atmospheric Chemistry and Physics, 24, 2129–2167, https://doi.org/10.5194/acp-24-2129-2024, 2024.
- Tsuruta, A., Aalto, T., Backman, L., Krol, M. C., Peters, W., Lienert, S., Joos, F., Miller, P. A., Zhang, W., Laurila, T., Hatakka, J., Leskinen, A., Lehtinen, K. E. J., Peltola, O., Vesala, T., Levula, J., Dlugokencky, E., Heimann, M., Kozlova, E., Aurela, M., Lohila, A., Kauhaniemi, M., and Gomez-Pelaez, A. J.: Methane Budget Estimates in Finland from the CarbonTracker Europe-CH4 Data Assimilation System, Tellus B: Chemical and Physical Meteorology, 71, 2019.
- Tsuruta, A., Kivimäki, E., Lindqvist, H., Karppinen, T., Backman, L., Hakkarainen, J., Schneising, O., Buchwitz, M., Lan, X., Kivi, R., Chen,
 H., Buschmann, M., Herkommer, B., Notholt, J., Roehl, C., Té, Y., Wunch, D., Tamminen, J., and Aalto, T.: CH4 Fluxes Derived from
 Assimilation of TROPOMI XCH4 in CarbonTracker Europe-CH4: Evaluation of Seasonality and Spatial Distribution in the Northern
 High Latitudes, Remote Sensing, 15, 1620, https://doi.org/10.3390/rs15061620, 2023.
 - Turner, A. J., Frankenberg, C., and Kort, E. A.: Interpreting Contemporary Trends in Atmospheric Methane, Proceedings of the National Academy of Sciences, 116, 2805–2813, https://doi.org/10.1073/pnas.1814297116, 2019.
- Virkkala, A.-M., Rogers, B. M., Watts, J. D., Arndt, K. A., Potter, S., Wargowsky, I., Schuur, E. A. G., See, C. R., Mauritz, M., Boike, J., Bret-Harte, M. S., Burke, E. J., Burrell, A., Chae, N., Chatterjee, A., Chevallier, F., Christensen, T. R., Commane, R., Dolman, H., Edgar, C. W., Elberling, B., Emmerton, C. A., Euskirchen, E. S., Feng, L., Göckede, M., Grelle, A., Helbig, M., Holl, D., Järveoja, J., Karsanaev, S. V., Kobayashi, H., Kutzbach, L., Liu, J., Luijkx, I. T., López-Blanco, E., Lunneberg, K., Mammarella, I., Marushchak, M. E., Mastepanov, M., Matsuura, Y., Maximov, T. C., Merbold, L., Meyer, G., Nilsson, M. B., Niwa, Y., Oechel, W., Palmer, P. I., Park, S.-J., Parmentier,
- F.-J. W., Peichl, M., Peters, W., Petrov, R., Quinton, W., Rödenbeck, C., Sachs, T., Schulze, C., Sonnentag, O., St. Louis, V. L., Tuittila, E.-S., Ueyama, M., Varlagin, A., Zona, D., and Natali, S. M.: Wildfires offset the increasing but spatially heterogeneous Arctic-boreal CO2 uptake, Nature Climate Change, 15, 188–195, https://doi.org/10.1038/s41558-024-02234-5, publisher: Nature Publishing Group, 2025.
 - Wania, R., Ross, I., and Prentice, I. C.: Implementation and Evaluation of a New Methane Model within a Dynamic Global Vegetation Model: LPJ-WHyMe v1.3.1, Geoscientific Model Development, 3, 565–584, https://doi.org/10.5194/gmd-3-565-2010, 2010.
- Ward, R. H., Sweeney, C., Miller, J. B., Goeckede, M., Laurila, T., Hatakka, J., Ivakov, V., Sasakawa, M., Machida, T., Morimoto, S., Goto, D., and Ganesan, A. L.: Increasing Methane Emissions and Widespread Cold-Season Release From High-Arctic Regions Detected Through Atmospheric Measurements, Journal of Geophysical Research: Atmospheres, 129, e2024JD040766, https://doi.org/10.1029/2024JD040766, 2024.
- Weber, T., Wiseman, N. A., and Kock, A.: Global Ocean Methane Emissions Dominated by Shallow Coastal Waters, Nature Communications, 10, 4584, https://doi.org/10.1038/s41467-019-12541-7, 2019.
 - Wittig, S., Berchet, A., Pison, I., Saunois, M., Thanwerdas, J., Martinez, A., Paris, J.-D., Machida, T., Sasakawa, M., Worthy, D. E. J., Lan, X., Thompson, R. L., Sollum, E., and Arshinov, M.: Estimating Methane Emissions in the Arctic Nations Using Surface Observations from 2008 to 2019, Atmospheric Chemistry and Physics, 23, 6457–6485, https://doi.org/10.5194/acp-23-6457-2023, 2023.

- Xu, J., Morris, P. J., Liu, J., and Holden, J.: PEATMAP: Refining Estimates of Global Peatland Distribution Based on a Meta-Analysis, CATENA, 160, 134–140, https://doi.org/10.1016/j.catena.2017.09.010, 2018.
- Ying, Q., Poulter, B., Watts, J. D., Arndt, K. A., Virkkala, A.-M., Bruhwiler, L., Oh, Y., Rogers, B. M., Natali, S. M., Sullivan, H., Armstrong, A., Ward, E. J., Schiferl, L. D., Elder, C. D., Peltola, O., Bartsch, A., Desai, A. R., Euskirchen, E., Göckede, M., Lehner, B., Nilsson, M. B., Peichl, M., Sonnentag, O., Tuittila, E.-S., Sachs, T., Kalhori, A., Ueyama, M., and Zhang, Z.: WetCH₄: a machine-learning-based upscaling of methane fluxes of northern wetlands during 2016–2022, Earth System Science Data, 17, 2507–2534, https://doi.org/10.5194/essd-17-2507-2025, publisher: Copernicus GmbH, 2025.
 - Yuan, K., Li, F., McNicol, G., Chen, M., Hoyt, A., Knox, S., Riley, W. J., Jackson, R., and Zhu, Q.: Boreal–Arctic Wetland Methane Emissions Modulated by Warming and Vegetation Activity, Nature Climate Change, 14, 282–288, https://doi.org/10.1038/s41558-024-01933-3, 2024.
- Zhang, Z., Poulter, B., Feldman, A. F., Ying, Q., Ciais, P., Peng, S., and Li, X.: Recent Intensification of Wetland Methane Feedback, Nature Climate Change, 13, 430–433, https://doi.org/10.1038/s41558-023-01629-0, 2023.